SSCL-N-697

TOROIDAL DETECTOR SCOPING STUDY

for the
Superconducting Super Collider Laboratory
Universities Research Associate, Inc.

Prepared by

Dr. James N. Luton, Jr.
Oak Ridge National Laboratory
Oak Ridge, Tennessee 37831-8040

and

Mr. Peter Bonanos
Princeton Plasma Physics Laboratory
Princeton University
Princeton, New Jersey 08544

under the direction of

Professor Michael Marx
State University of New York at Stony Brook
Department of Physics, High Energy Group

Table of Contents

	Page
Introduction and Summary	3
Magnet Requirements and Geometry	3
Toroidal Coil Mechanics	4
Conductor Selection	6
Winding the Octants	13
Toroid Dimensions	13
Structural Models	14
Properties of the Structural Aluminum	19
Magnetic Field Shape Considerations	20
Assembly	21
Commentary	21
References	22

Appendix A (Toroidal Coil Mechanics)

Appendix B (Nastran Model and Results)

Appendix C (Magnetic Field Plots)

Appendix D (Coil and Structure Weights and Sizes)

Appendix E (Cost Data - Fusion Magnets)

INTRODUCTION AND SUMMARY

The feasibility of constructing air-core toroidal bending magnets for use as detectors for the SSC is summarized and a design is described and analyzed. The requirement that a bending length of 4 T-m be provided in a toroid which encloses a calorimeter is achieved using criteria which are more conservative than those of operating superconducting toroids.

The design and construction is clearly feasible.

The superconducting toroids which have been built for thermonuclear fusion experiments serve as reference designs. Detector magnets, by comparison, offer considerably more freedom in available design options and many of the variants have not been considered or included in this study. A conceptual design effort and a conductor development effort are recommended, and a suggested list of further work is provided. Additional effort may produce substantial improvements to the design.

The magnets described here require a construction time of 3.5 years and a Title I design phase of 1.8 years. The recommended efforts are aimed at improving the performance and reducing the cost. The construction period would probably not be shortened. A table of component weights is provided to be used for cost estimates.

MAGNET REQUIREMENTS AND GEOMETRY

The toroid surrounds a calorimeter nominally 6 m in diameter and 15 m in length. If the necessary bending power is 4 T-m the required volume of toroidal magnetic field has the form of Fig. 1.

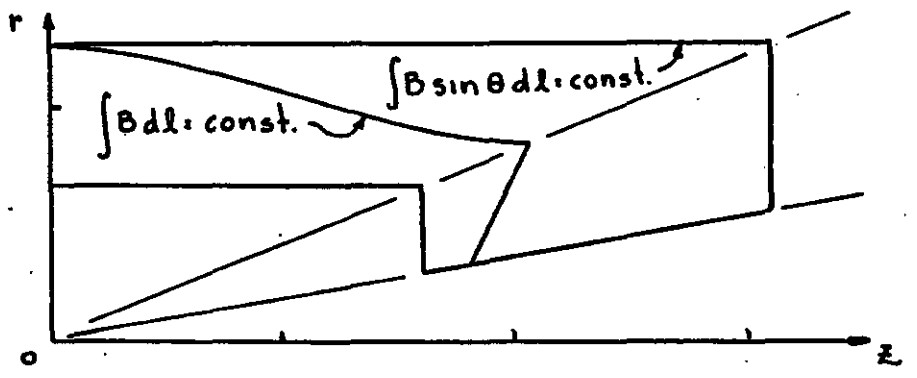

Fig. 1. Required Field Volume

A rectified, intermediate form of this volume may be produced using the following arrangements, and designated as shown.

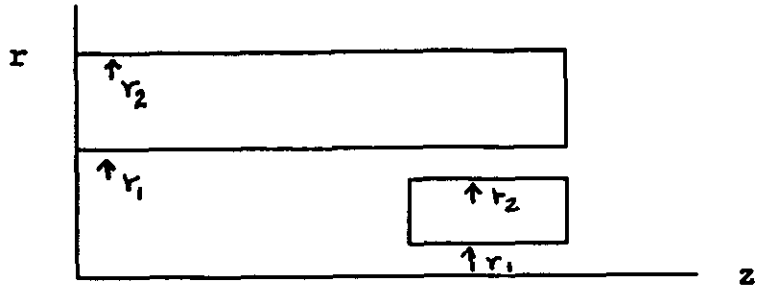

Fig. 2. Central Toroid with End Plug

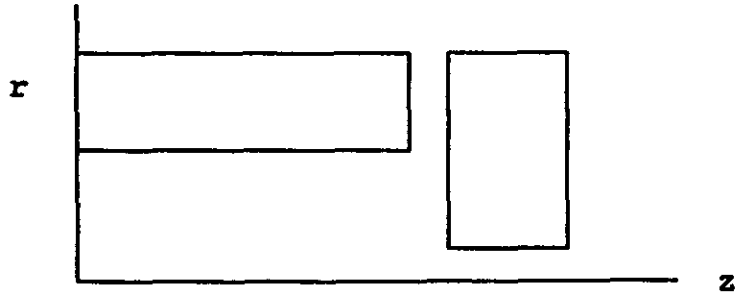

Fig. 3. Central Toroid with End Cap

Both arrangements are evaluated. For reasons explained later, the arrangement in Fig. 2 is preferred on the basis of magnet structural considerations alone and the Fig. 3 configuration is preferred when the chosen superconductor bending radius and compatibility with the calorimeter support are the major factors. On balance, the recommended arrangement is the Central Torus with End Caps.

TOROIDAL COIL MECHANICS

The Lorentz force (Fig. 4) on an element of an ideal thin toroidal shell is a magnetic pressure normal to the shell and directed outward, away from the field volume. The force sum may be considered as having two components; an axial force separating the torus and, for each sector, a radial centering force. The axial force is a function of the inner and outer radius and the field strength. It is independent of the shape of the path between radii [1 and Appendix A]. The centering force is shape-dependent.

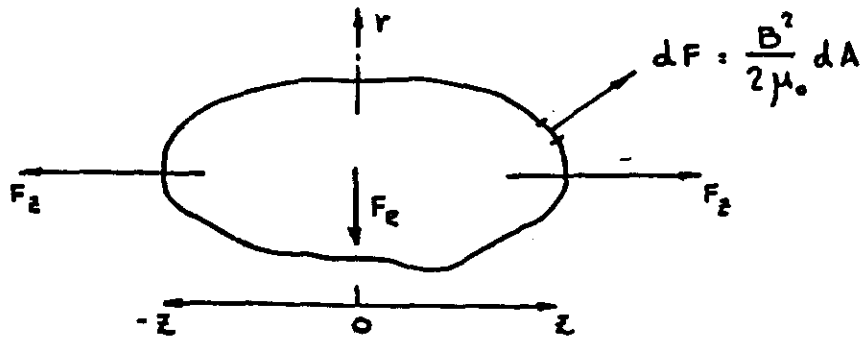

Fig. 4. Idealized Toroid

The sum of all forces is zero; the magnetic loads of a superconducting torus may therefore be supported by cold structure alone. External supports to the warm environs are required for gravity loads, seismic effects and the relatively minor loads resulting from interaction between nearby imperfect toroids. Imperfect here means toroids with gaps and, hence, leakage fields.

Structurally efficient toroids are shaped such that they are stressed uniformly throughout the structural volume with little or no bending. If a toroid is composed of an array of structurally independent planar coils a bending-free shape is obtained if the product of the curvature and line pressure is constant between r_1 and r_2 [2,3,4]. If the conductor/structure is arranged such that it is capable of supporting tensile forces in both the toroidal and poloidal directions (a shell structure) then a constant tension surface may be considered provided that the aspect ratio r_2/r_1 is low enough.

Efficient structures are however, at odds with the field requirements for a detector (Fig. 5). Their utility is in understanding the distortion of all other shapes which, under load, deform such as to approach these minimum energy, ideal shapes.

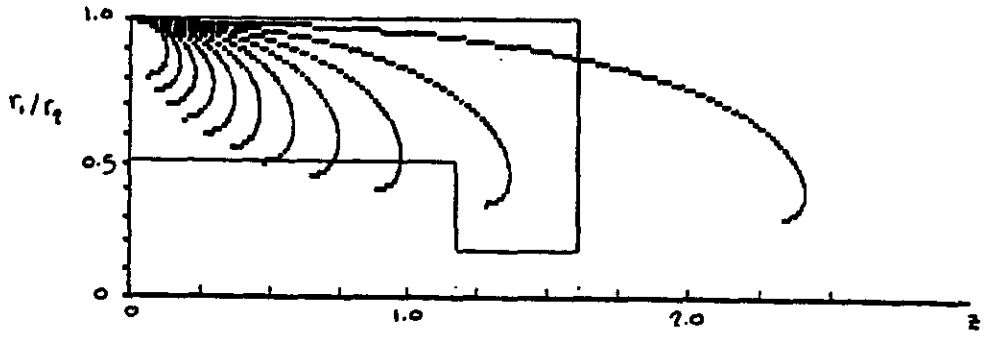

Fig. 5. Constant Tension Shapes

The centering force tends to buckle the central supporting cylinder at r_1. This tendency is aggravated if the conductors at r_1 and r_2 are not tied together structurally along their respective axial lengths, i.e., the force at r_1 is radially inward and the force at r_2 is radially outward. The toroid contains wire chambers and electronics within the field volume and pathways for maintenance access are required. Additionally, the magnet encloses a calorimeter which requires exit paths for instrument leads. The toroid must, therefore include gaps at several azimuthal positions and along its length. These gaps further aggravate the buckling tendency since the loads applied to the central cylinder are now localized as linear bands of force which indent the cylinder.

In summary, the configuration chosen to demonstrate feasibility is a planar-end torus with large gaps between coil windings and an "open" interior with no structural connections between the inner and outer conductor paths except at the end faces.

Interior supports, corner radii or reinforcement and reduced gap size are simple improvements to this structural worst-case.

CONDUCTOR SELECTION

The various choices leading to a conductor selection need not be optimal, but the resulting conductor should meet the requirements dependably without throwing undue burdens on other parts of the system. The logic for these choices is described below, and summarized in Table 1.

Table 1. Conductor Choices (Underlined)

1. <u>NbTi</u> vs Nb_3Sn

2. Subatmospheric temperatures? Yes or <u>no</u>

3. Pool boiling vs <u>forced flow</u>
   - 15 or 21-m horizontal lengths of conductor in high field region
   - small-scale experiments more dependably extrapolated
   - higher voltage withstand capability

4. <u>Cable</u> vs load-bearing subelements
   - greater stability margin

5. <u>One</u> sheath vs two
   - helium access
   - cost

6. All copper in MF strands vs <u>some all-copper strands</u>
   - use developed SSC strands (Cu/SC = 1.8)
   - need additional copper for quench protection only
   - separate copper less costly

The superconductor material selected was NbTi, since it was considered that Nb_3Sn is not yet really commercial. It also seemed better not to be restricted by its strain sensitivity. The operating temperature of 4.5 K was selected high enough that the refrigerator need not operate at subatmospheric pressures and be at risk to inleakage of contaminants, even though this choice reduces somewhat the critical current of the superconductor.

Conductors are usually classified as "pool boiling," in which any heat produced in the winding is removed by boiling of the liquid helium in which it is immersed, or "forced flow," in which the heat is removed by flowing helium confined within the conductor. In the case of high performance pool-boiling coils, as the coil becomes larger it becomes more difficult to reliably extrapolate its cooling and performance from small-scale tests on heat transfer and bubble removal. Also, the helium is depended upon for voltage withstand during dump, just when it is being heated, and this limitation is more important as the magnet size and stored energy increase. In our particular geometry the long thin horizontal legs tend to give less effective natural circulation. Finally, the different orientation of the octants with respect to gravity mean that with a pool-boiling design neither the octant windings nor their dewars could be identical. A forced-flow design was chosen.

Forced-flow conductors can be classified according to whether their internal current-carrying members will support major transverse loads, or whether these loads are borne mainly by the sheath. The latter "cable-in-conduit" configuration was selected, primarily because of its large cooling surface and stability margin, but also because it is considered less expensive. An arrangement with multiple sheaths can offer larger hydraulic diameter and lower pressure drops, but a single sheath arrangement is nearly as effective and was selected to lower costs and to permit direct access to the helium through a single sidewall.

Because the conductor sheath is captured by a structure with somewhat different thermal expansion, because of the application of transverse magnetic loads and their transmission from one conductor to another (this is the largest load), and because of the internal pressure and temperature gradients during quench, the conductor is an important and highly loaded structural member. This is summarized in Table 2. Initial hand calculations of stress in the sheath showed combined stress above 150 ksi even with the corner outer radius only twice the wall thickness. There are several ways to reduce the sheath stress, and future work should examine them carefully.

The conductor would look very similar to the conductor of Fig. 6, which was used successfully in the coil of Fig. 7. Part of an international program for coil development called the Large Coil Task (LCT) [5], this coil was installed with five other coils to form a toroidal array, as shown in Fig. 8. This toroid was the prior art nearest to the toroids investigated herein. It had six different coils of 2.5- x 3.5-m bore, which reached 9-T peak field with 946 MJ total stored energy, $\approx$2.4 to 3.9 kA/cm^2 in a winding pack and overall current density in the nose regions of 1.5 to 1.8 kA/cm^2.

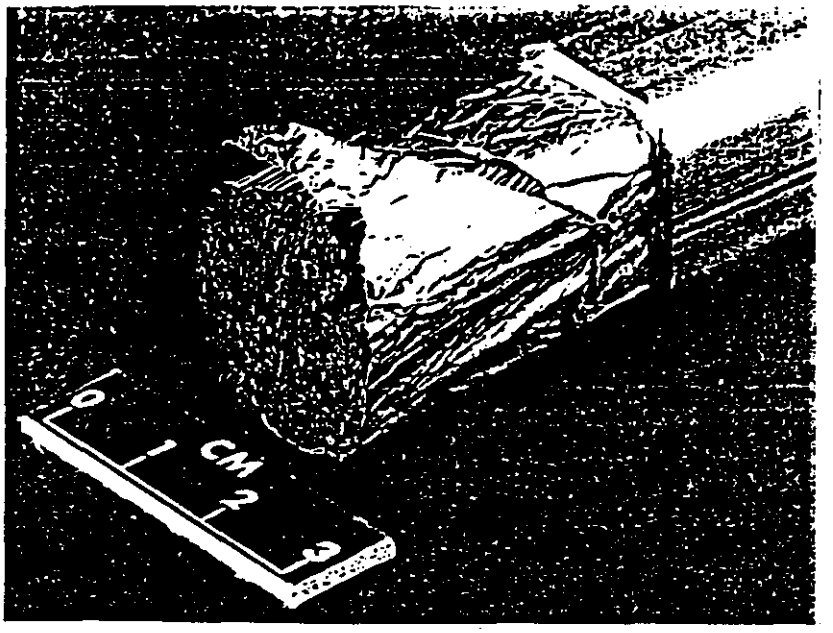

FIG. 6. Conductor produced by Airco for the Westinghouse-LCT coil, showing the 6 x 3^4 multifilamentary Nb_3Sn strands, the protective foil wrap, and the JBK-75 sheath with longitudinal closure weld.

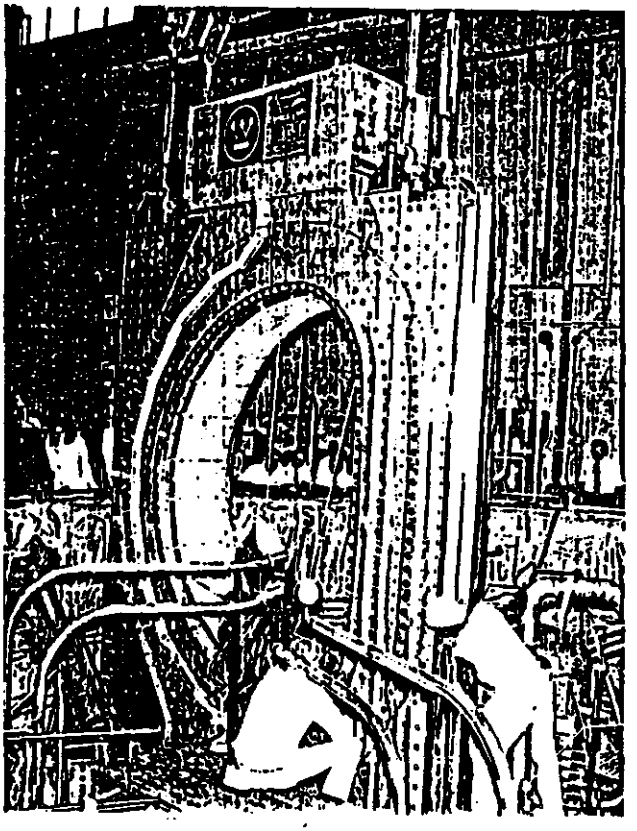

FIG. 7. Westinghouse-LCT coil being lowered into the vacuum vessel.

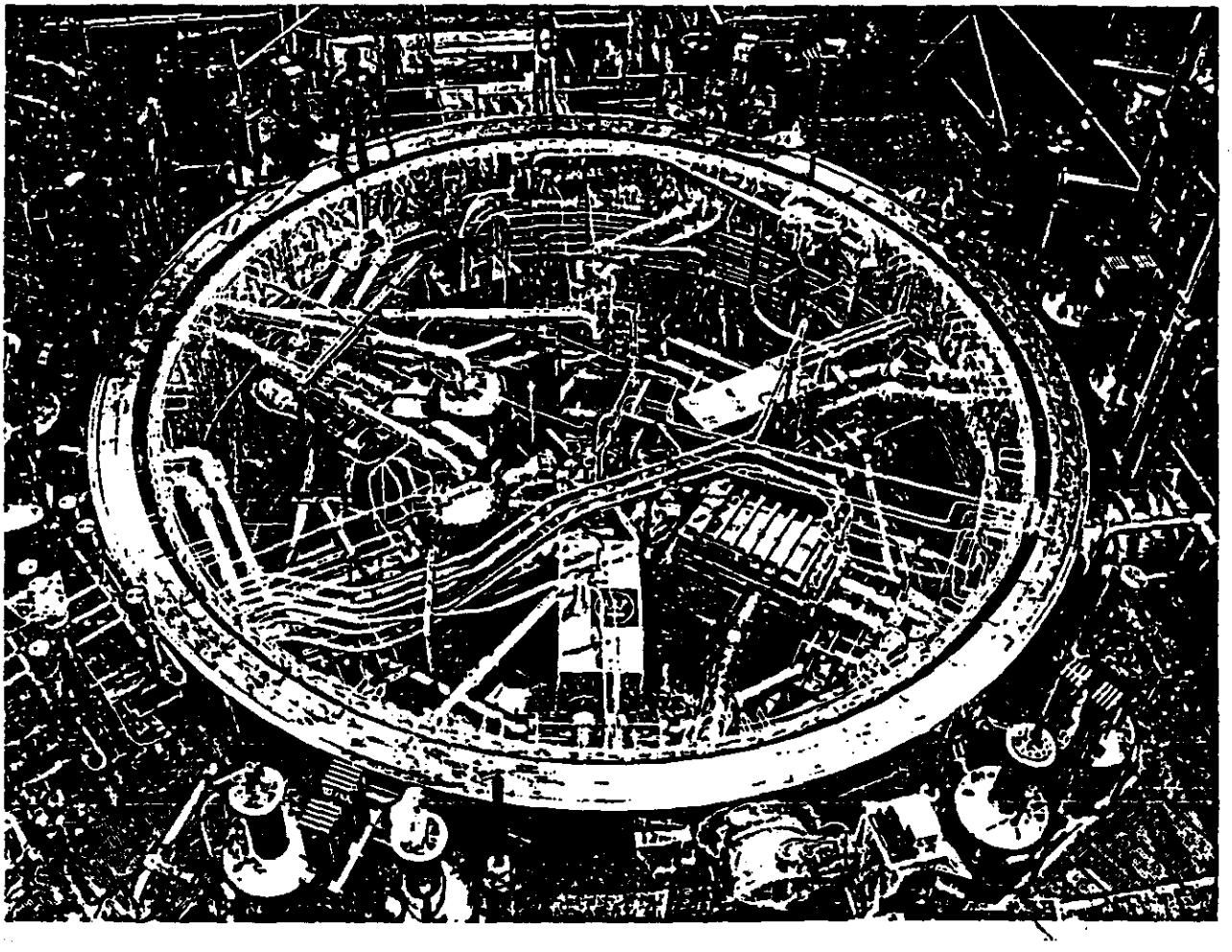

FIG. 8. LCT vacuum vessel before installation of lid, showing the six coils mounted against the bucking post.

Table 2. Sheath Loads

After fabrication of conductor and coil, the conductor sheath must withstand the simultaneous loads due to

- thermal shrinkage on cooldown —
  SS vs Al: $\epsilon = (415 - 290) \times 10^{-5} = 1.25 \times 10^{3}$ longitudinal compression.
  $\sigma > 34$ ksi

- unequal heating due to quench —
  moderated by induced currents.

- magnetic loads —
  2000 psi overall, vs 7250 for ALCATOR DCT. Sheath stress is ≥150 ksi, but is reducible by epoxy potting, square outer corners, or reduced size.

- quench pressure —
  controllable by conductor design and flow path length.

Yield stress at 4.2 K:

Annealed 316 LN or 304 LN ≈150 ksi (McHenry & Reed); Nitronic 40 ≈200 ksi (Westinghouse Phase I Report)

The final choices listed in Table 1 concern the individual strands comprising the conductor cable. The strands for the outer layer of the SSC dipole magnets are most attractive, because they are well developed and characterized, and of suitable diameter (0.0255 in.), residual resistivity ratio (89), and critical current density in the NbTi (242 kA/cm^2, 2420 A/mm^2) for satisfactory current and stability. However, at their copper to superconductor ratio of 1.8 they would not provide sufficient copper to keep temperatures and pressures at safe levels in case of the quench of a coil with so much energy stored in the field. Therefore, a cable was selected with pure copper strands in addition to the multifilamentary (MF) superconducting strands. It is much less expensive to provide copper in separate strands than in a composite, and its resistivity ratio can be larger. In order to reduce the risk of damage of the NbTi and to ease the fabrication of coolant connections, enough of the copper strands would be put around the MF cable core to completely cover it.

Figure 9 is a sketch of the conductor, at a cross section taken through a helium connection. The hole for helium access is drilled during fabrication of the magnet, after the conductor itself is completed, at any point along the conductor where access is needed. This eliminates the need of fabricating the conductor in short accurate lengths, or of predicting how much the conductor length will increase during coil fabrication. The cable itself is not disturbed, except that in "drilling" the hole, for example with an end mill while the cable space is pressurized with dry gas, one is allowed to cut into the outer copper strands as the foil sheath is penetrated, since this would not affect the performance of the coil. Cable ends and the electrical joints they necessarily entail are rare, their number being determined only by shipping and material handling considerations.

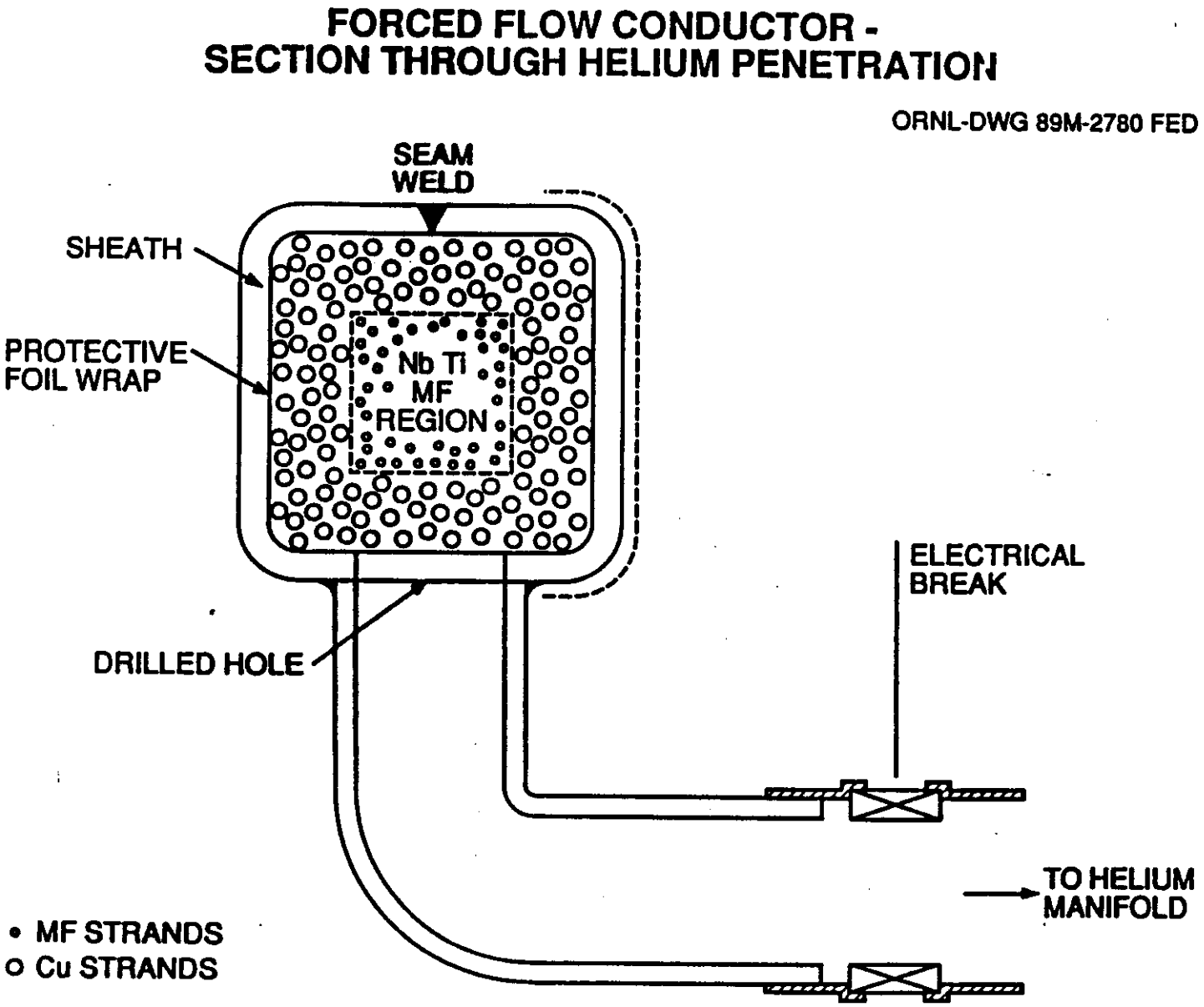

FIG. 9. Conductor cross section, taken at a helium exit. Sheath, allowance for electrical insulation, and helium tube shown to scale (width across flats including insulation, 1.3 in.). Cable region and electrical break are shown schematically.

As indicated in Fig. 9, an "electrical break" is required at each helium connection, since the helium is brought to the winding in metal tubes which are at ground potential. These breaks may be ceramic or fiberglass-epoxy, but in either case the details of the design must be proper, straining of the insulator avoided, and leak checking carefully done. The weld joining the helium tubes and the conductor sheath must also be carefully designed and executed. Although not as massive as the sheath seam weld, melt-through of the foil is still a consideration, both because this weld is done after the sheath is tightened about the cable and because the geometry may not be well suited to the use of automated welders. Earlier tests [6] (but with smaller tubes) indicate that the sheath is not appreciably weakened by the combination of a drilled hole reinforced by a welded tube; when pressurized with a cryogen, the rupture still occurred at a corner rather than at the drilled hole.

Helium inlets and outlets alternate along the conductor with the flow paths in parallel. Thus a flow path is from inlet header through a tube and an electrical break to a drilled sheath penetration, across the strands to fill the cable interstices, it then splits and flows both directions down the cable to the adjacent penetration, where it joins flow from the other direction and exits through the electrical break and exit header. Each penetration represents a halt of the winding line while the insulation is removed locally, the hole fixtured and drilled, the preformed elbow welded on and leak checked, and new insulation applied. Therefore to control costs the number of penetrations should be minimized and the length of flow path maximized. Conductor stability is not a factor; the only limitations on flow-path length are gross heat removal and increase in sheath stress due to the quench-induced pressure rise which occurs while the magnetic load still exists. The pressure rise is decreased by the additional copper in the cable, and the steady-state heat to be removed by the cable flow is kept low by good thermal isolation (or by auxiliary flow paths in the structure) and by having few electrical joints in the strands and cable.

Airco first developed the fabrication of the conductor of Fig. 6 using Nitronic 40 as the sheath material. This strong stainless (200 ksi yield strength at 20 K) usually has properties suitable for cryogenic service, but was abandoned because the peculiar fabrication sequence required for the sheath of the Nb_3Sn conductor ruined its toughness. The NbTi conductor needs no post-sheathing heat treatment, and Nitronic 40 is the material of choice.

Joining of the individual strands with butt welds is established technology. The technology of joining the full conductors end-to-end was developed for the Westinghouse LCT coil. Although quite tedious and therefore expensive, the process provides a helium connection at the joint, is reasonably compact, and proved reliable in service. Test data indicated $1.3 \times 10^{-9}\ \Omega$ at 2 T and $2.6 \times 10^{-9}\ \Omega$ at 6 T for an 18-kA, 486-strand cable. These are acceptable values, and would give about 2 W per joint in our case. This is a pessimistic estimate, since when used with a NbTi cable the conductance per unit area of such joints should be still higher.

Table 3 describes the conductor for the end toroid, where the field at the conductor is 6 T. This conductor was given more consideration than the 2-T conductor for the central toroid, since if the 6-T case is feasible the 2-T case is also feasible---if desired, one could simply use the same conductor, although the optimal 2-T conductor would have less superconductor and more copper. Both values of the fifth entry of Table 3 are for the benefit of the cryogenic system, and the value chosen for the pressure has little influence on the conductor. A rather large current (40 kA) was desired to keep the quench voltage down and the conductor size appropriate for fabrication of such

a large coil. The disadvantages of the large current are a factor of two extrapolation from past experience, a larger minimum bend radius (estimated at 50 cm), and a larger span for the sheath walls (which act as eccentrically loaded columns when restraining the magnetic crushing loads). Although the 40 kA is feasible, subsequent studies may determine that a different value is optimal.

Table 3. Forced-Flow Conductor for SSC Toroidal Detector

Type

Cable-in-conduit, with NbTi multifilamentary strands surrounded by some copper strands

Sheath - Nitronic 40 stainless steel, formed from 0.1-in. strip; formed and seam welded
Helium Penetrations - made at any location as needed, during fabrication of the coil
Field - 6 T
Helium - 4.5 K, 5-atm, single-phase
Current - 40 kA
Cable Space - 25-35% helium, remainder strands
Overall Cu/SC - 9.1
Current Density - over the "active" cable space - 21.0 kA/cm^2
over the cable space - 5.86
over the conductor - 3.74

Strands

MF NbTi: (SSC "outer layer" strands)

Cu/SC - 1.8
RRR - 89.0
j_c - 250 kA/cm^2 over the NbTi, at 5 T and 4.2 K
Diameter - 0.0255±0.001 in.
Twist - 2 per inch, clockwise
Number - 401

Copper:

Diameter - 0.051 in.
Number - 262
Material - OFHC
Temper - seller's option
RRR - ≥89.0

At Operating Conditions

Stability margin ≈ 250 mJ/cm^3 of strands
Limiting current/operating current - ≈1.1
Operating current/critical current ≈ 0.50
Pressure rise if whole 100-m length quenches - ≈150 atm (2200 psi)

The copper to superconductor ratio is given in Table 3 for interest only; as long as the areas of copper and superconductor are suitable this ratio is of little consequence and should be considered a dependent variable. The current density over the conductor (3.7 kA/cm^2) happens to be similar to that for the Westinghouse LCT coil (3.9 design value, 5.1 achieved). In the table "cable space" refers to the total area inside the sheath, and "active cable space" is the area of the MF strands and their associated helium. This distinction is made because although the quench pressure calculation assumed all the copper carried current during a quench, the stability calculation assumed that the time span for recovery was so short that the only effective copper was that of the MF strands. This latter may not be true, since the strands will not be deliberately insulated, but it is conservative.

The strand data of Table 3 was simply taken from the SSC strand specifications, and the number of strands set to give the desired total area of NbTi. The table shows MF and copper strand data as though they were independent. Actually some copper strands would be added with the MF strands to give a suitable number for cabling, probably 486 (6 x 3^4). These strands would be worked to have the same diameter as the MF strand and similar mechanical properties. The remaining copper would be in strands whose diameter and temper would be suitable for cabling about this core cable.

The stability margin is defined as the largest sudden input of heat per unit volume of conductor that the magnet can withstand without quenching. The stability margin required for dependable operation is an unsettled point. The detector toroid is quite different from the SSC dipoles: very high current densities are not essential, substantial mechanical heat inputs are not avoidable, and the loss of a single coil (octant) is not tolerable. Thus its stability margin must and can be much higher than for the dipoles. Table 4 shows the basis for choosing a stability margin of 150 mJ/cm^3 as a design criteria.

Table 4. Required Stability Margin

- In stability tests on the Westinghouse-LCT coil (unpotted, Nb_3Sn), it withstood a sudden heat input of at least 1000 mJ/cm^3 of strands (25 K) and recovered. It never spontaneously quenched.
- The EURATOM-LCT coil (potted, NbTi) was thought to have a stability margin of about 100 mJ/cm^3, and never spontaneously quenched.
- The Swiss-LCT coil (potted, NbTi) had a still lower stability margin, and spontaneously quenched six times.
- Potted, glued, and friction-held LCT coils showed acoustic emission---some coincident with conductor motion.
- Recent attempts at measuring thermal effects of epoxy cracking indicate $\approx$70 mJ/cm^3. (Yanagai, *Cryogenics*, July 1989).
- Choose to design to q > 150 mJ/cm^3.

The last portion of Table 3 shows the operating conditions. The "limiting current" is the current at which the stability margin abruptly decreases, by perhaps an order of magnitude. The 1.1 current ratio shown is uncomfortably small, but it should be little trouble to increase it in the next iteration. The 0.5 ratio is conservative. The pressure rise was calculated assuming that the whole length of flow path either quenches initially or (by "thermohydraulic quenchback") very soon thereafter; thus the listed pressure represents an upper limit. It is thought that substantial reductions could be obtained in costs of conductor and magnet fabrication if the stability and quench pressure characteristics were better known by conductor tests and comparisons with theory before the toroid design were finalized.

Figure 10 shows graphically the tradeoffs [7,8] involved in apportioning the allowed space among various constituents. The upper boundary is fixed by the NbTi, the left boundary (limiting current) by the heat-induced flow, and the right by the sheath strength. Since the calculations are approximate, the designer should not approach too closely any of the boundaries.

The quench pressure calculation assumed for simplicity that the current did not decrease in the time required for the pressure to reach a maximum. However, in our case we have provided an aluminum structure rather than steel, and it closely surrounds the winding. With electrical continuity provided by welding (even if the structural joints are bolted) then a closed path of conducting metal exists into which current can inductively transfer from the winding when the dump breakers actuate. The effect depends on the inductive coupling coefficient and on the L/R time constants of the structure and the coil circuit. Fig. 11 shows the measured and calculated results for a dump of the Westinghouse LCT coil [9], which inadvertently had its aluminum structure well shorted. The abrupt drop of 25% in current (50% in resistive power dissipation) is quite useful for reducing the maximum pressure and temperature reached on quench. If we limit the temperature to 120 K in order to limit strains due to unequal heating, and assume the Westinghouse LCT values for the coupling and L/R of the structure, the required dump voltage is only 720 V (Table 5), which is considered modest for a forced-flow coil.

Table 5. Quench Protection

- Issues are hot-spot temperature, quench pressure, and maximum dump voltage.

  With 1.35 GJ in the central torus, 25% of the 40-kA operating current transferring to the structure, a dump resistor of 18 mΩ, all turns in series, and with immediate detection and dump,

  T_{HS} = 120 K design choice.

  $P_q \leq$ 150 atm for 100-m flow path. Impacts allowed path length

  V_d = 720 V

  τ_d = 67 s

  Next design iteration could reduce T_{HS}, raise V_d, and probably should reduce area of copper strands.

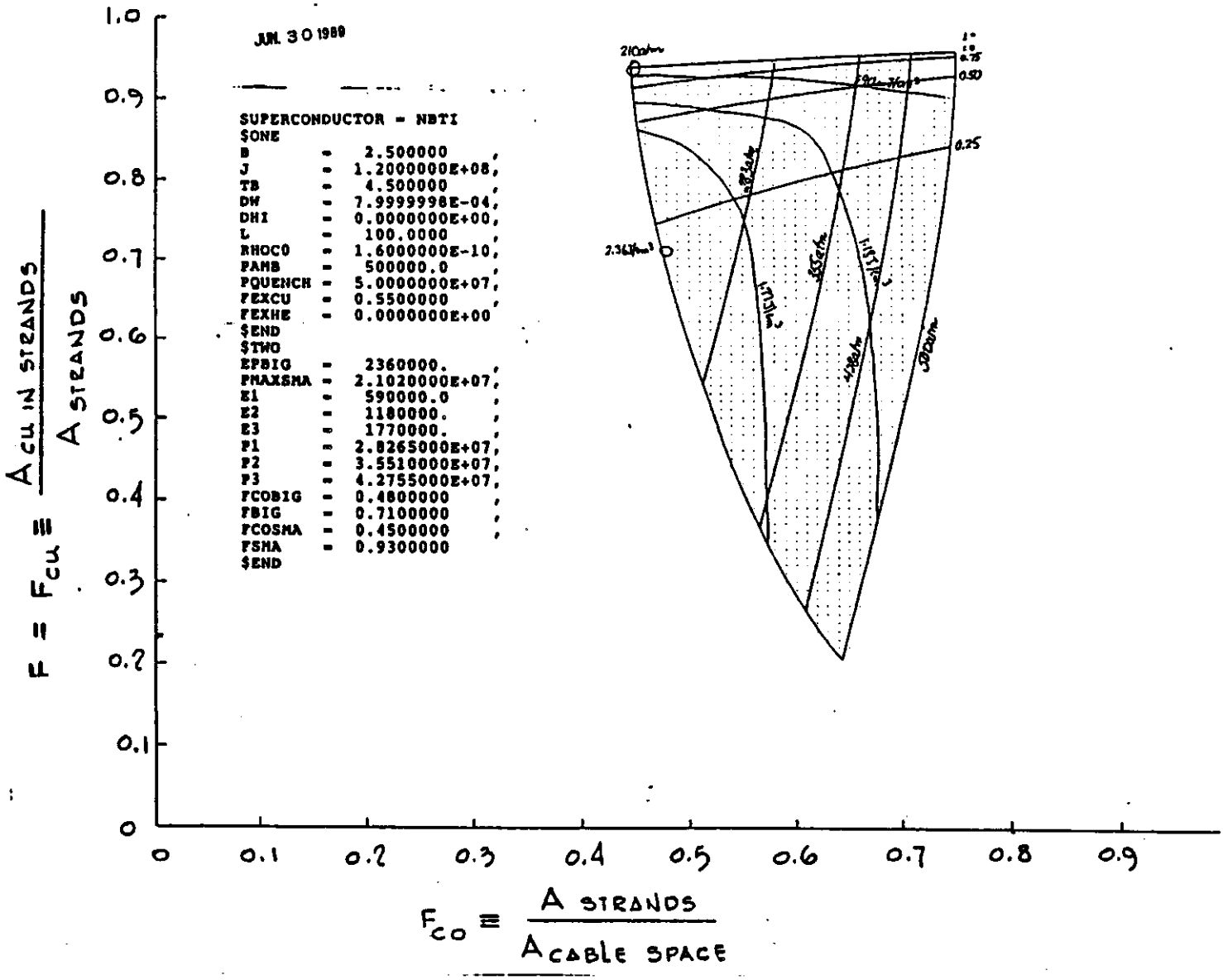

FIG. 10. Sample design space for a 6-T configuration with added "extra copper" = 55% of the cable space. Contours are of current ratio I/I_c, stability margin in J per cm³ of strands, and quench maximum pressure in atm. "Cable space" refers to the MF strands and associated helium; strand refers to MF strands only. "Extra copper" is presumed added by copper sheath or separate strands.

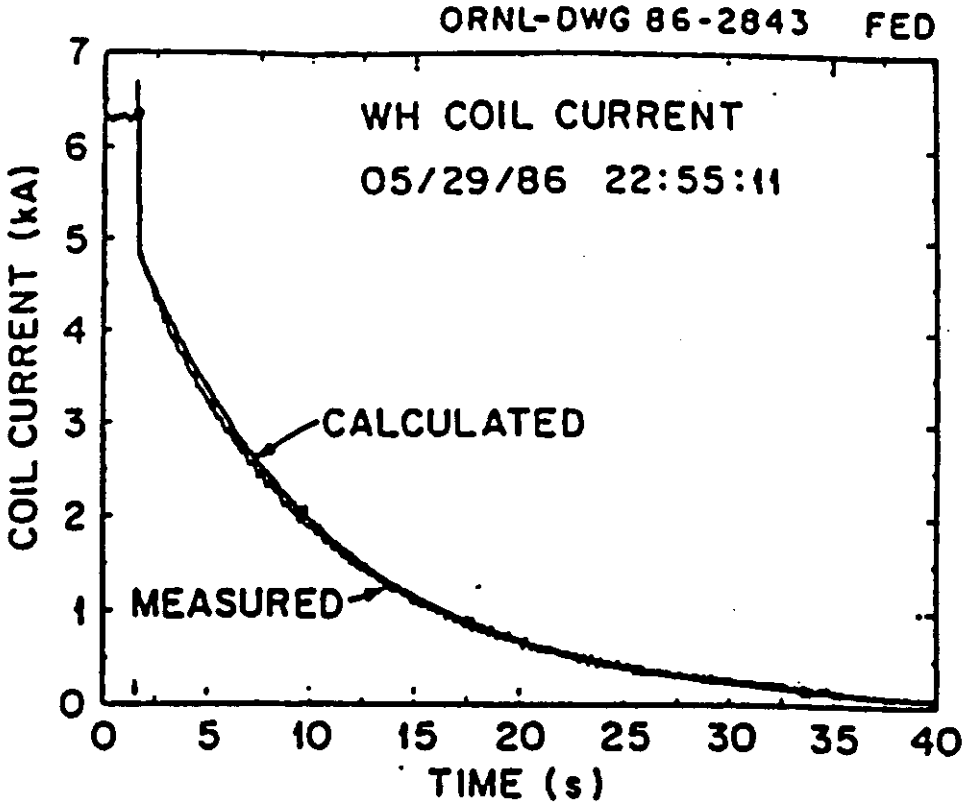

FIG. 11. Dump of the Westinghouse-LCT coil from 6400 A.

WINDING THE OCTANTS

As shown earlier, the conductor is to be placed in cavities formed in the aluminum structure. The octant structure may be placed on a turntable whose axis of rotation itself can be rotated about an axis coincident with the "SSC beam axis." This requires a large winding machine (the MFTF used a converted naval gun turret), but the conductor payout spool can then be fixed and a traveling winder is not required. If the shape of a turn stays a rectangle with small-radius corners, the bends at the corners will spring back (and perhaps also creep) so that overbending will be necessary. Sharp bends made on an insulated conductor will also be hard on the tape insulation, so that either an outer sacrificial tape layer will be needed, or the taping machine will be located to apply the tape after the bends are made. Standard practice is to tension the conductor to produce the bending as the structure (i.e., mandril) is rotated. One or more follower rollers applying radial pressure would probably be required, as would removable smaller-radius bending blocks. An alternate method would be to bend the conductor with two sets of 3-point bending jigs that move alternately along the conductor in crabwise fashion. One set moves while the other holds the bend, thus avoiding the tendency of the conductor to "flap" with each application and removal of the bending load. An advantage of this method is that each of the pressure "points" is a finite-area pad which does not slide across the insulation while loaded. This should cause less trauma to the insulation than the line pressure of a roller or the mandril itself.

Although for simplicity a single cavity for the octant winding was considered, in practice the cavity probably would be divided by radial teeth into several smaller cavities. When the winding is complete the outer shell of the structure would be installed and mechanically fastened to the mandril at the ends of the octant and at every tooth. This subdivision allows fewer turns per cavity, thus holding them more securely and preventing the accumulation of azimuthally compressive magnetic loads from one section to another. It also allows the inner and outer shells of the structure to act as a single cross section with a much larger moment of inertia, much like a honeycomb structure, and so to better withstand buckling loads.

In a toroidal magnet, the circumferential width available for the winding is approximately proportional to major radius, although the number of conductors contained must be the same. Thus if the toroid windings were of equal depth at the inner and outer legs r_1 and r_2, then at the outer leg only about r_1/r_2 of the circumference would be covered, and the remainder would be gaps. For all three of our toroids the ratio r_1/r_2 is large enough (from 2 to 6) that the wasted space is appreciable. To reduce this waste we would use the end flanges for transition regions and have a smaller number of layers at r_2 than at r_1, with more turns per layer. There are certain restrictions to be met, so that there is no net current azimuthally around either end flange (to avoid stray fields) and that the electrical leads can always be run as opposing pairs. However, there are ample suitable combinations. Figure 12 is a model showing several cases; the 6 to 1 case is also feasible.

TOROID DIMENSIONS

For both configurations considered here, the radial build of the central torus is the same and begins with a radius of 3 m at the first surface of the innermost dewar wall. Vacuum gaps of 8 cms are interposed between the liquid-nitrogen-traced superinsulation, the dewar warm walls and the cold structure; the gap dimensions are chosen to permit easy assembly and provide reasonable

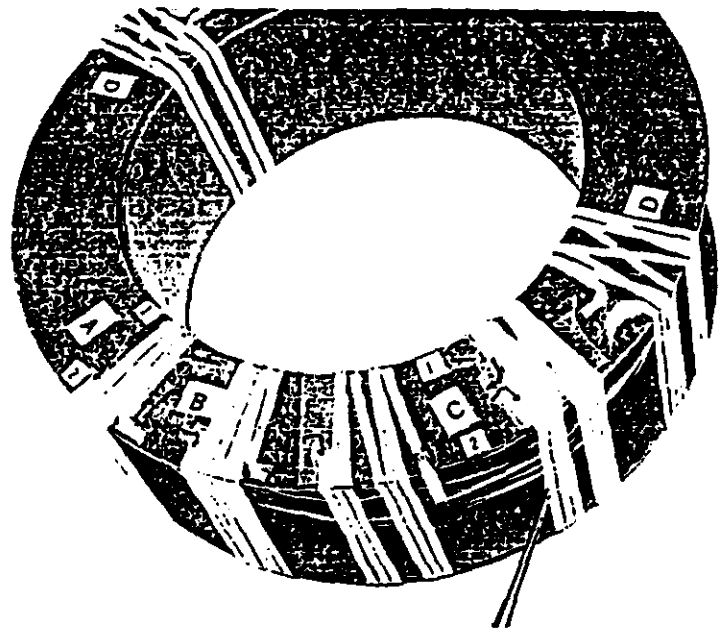

a.

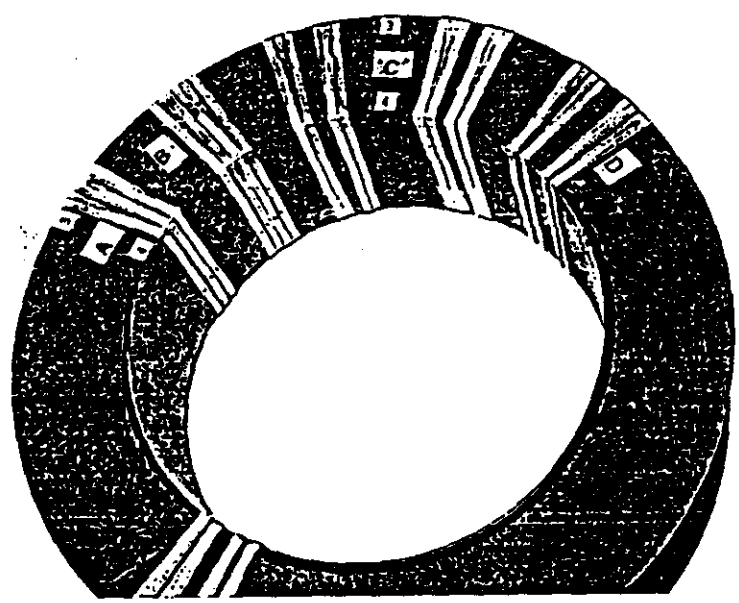

b.

FIG. 12. Photo showing some winding arrangements for use with different r_2/r_1 values. (a) obverse; (b) reverse. *C-right* shows a completed 3/2 segment; *C-left* shows the first layer before being covered by the second. *A* and *B* show the first half of 4/2 and 6/4 segments. *D* shows a completed 2/1 segment. Sequential numbers show the winding direction. Gaps in *C* and *D* are for structural teeth.

construction tolerances. The structural thicknesses are initial estimates based on a factor of at least two on the critical pressure for buckling for compressed cylinders such as the outer dewar walls and the central structural cylinder. The resulting outer radius is 7.5 m when all components and tolerances are included. A listing of dimensions along with a schematic diagram is provided (Table 6). This list, when read as shown applies to a central torus with a forward plug torus. The dimensions of an end cap (large forward torus) are given in the same pair of tables by combining radii 1 through 12 of the plug toroid with radii 15 through 26 of the central torus. The axial length of the central torus is 15 or 26 m depending on the configuration and the end torii are each 3 m long. The torus is divided into octants.

STRUCTURAL MODELS

The tabulated dimensions of Table 6 were then used to construct NASTRAN finite-element structural models. The code used to generate the model also computes the magnetic field at the coil surfaces; the resulting Lorentz forces are then applied as pressure loads on the elements which comprise the model. The elements (CQUAD4) within the cylindrical portions of the structure vary in thickness. The coil conductors are placed in grooves or pockets running axially along the cylinder surface. At the longitudinal sides of these pockets the thicker cylinder forms a wall. This feature provides a lateral (tangential) support for the coil winding during assembly and, as well, for a fault condition corresponding to any uneven distribution of current in any of the coils which would produce a lateral load. At both the pocket walls and inner-octant joints the elements are not only thicker but include offset centroidal planes in order to properly compute the plate bending moments.

The coil structural material is an aluminum alloy designated 2219-T87. Aluminum is chosen for the economy in forming and machining it offers and its good electrical conductivity; it may serve as a current path in the event of a quench. This alloy is well documented and mechanical properties at cryogenic temperatures appear in the Handbook on Materials for Superconducting Machinery. The strengths are adequate for this application. A summary of properties is included below. This material was used for the structure of an LCT coil and has performed well. The dewar walls are sized based on austenitic stainless steels since field welds are required for assembly and these materials may be easily fused to produce vacuum-tight joints. This choice may be modified however if a radiation "thin" design is desired. The octant joints may be bolted using A-286 fasteners (40% CW and aged).

The models were evaluated using MSC NASTRAN version 65B on the Cray-1 ("D" Machine) at the National Magnetic Fusion Energy Computer Center (NMFECC) at the Lawrence Livermore National Laboratory (LLNL). The models were generated on an IBM Personal Computer which is also a terminal connection to the NMFECC via the CTSSLINK software package. The output files are processed using both LLNL and PPPL software to produce graphic output as well as numerical tabulation of stress and displacement values. The basis of the models and a few important results are presented in the following tables.

TABLE 6

TOROID DIMENSIONS

TABLE OF DIMENSIONS - CENTRAL TORUS
Radial Line, Midplane of Octant
Basis:
Bending Length= 4 Tesla-Meters
NI of System= 30 MegAmp-turns

Meters		Inches		Meters(cold)		
r	dr	r	dr	r	dr	
3.000	0.020	118.110	0.787	3.000	0.020	1
3.020	0.080	118.898	3.150	3.020	0.072	2
3.100	0.080	122.047	3.150	3.092	0.080	3
3.180	0.080	125.197	3.150	3.172	0.075	4
3.260	0.200	128.346	7.874	3.247	0.199	5
3.460	0.070	136.220	2.740	3.446	0.069	6
3.530	0.025	138.961	0.984	3.516	0.025	7
3.555	0.080	139.945	3.150	3.540	0.085	8
3.635	0.080	143.094	3.150	3.625	0.080	9
3.715	0.080	146.244	3.150	3.705	0.089	10
3.795	0.025	149.394	0.984	3.795	0.025	11
3.820	0.315	150.378	12.390	3.820	0.315	12
4.134	1.935	162.768	76.194	4.134	1.935	13
6.070	0.500	238.962	19.689	6.070	0.500	14
6.570	0.040	258.650	1.575	6.570	0.040	15
6.610	0.080	260.225	3.150	6.610	0.063	16
6.690	0.080	263.375	3.150	6.673	0.080	17
6.770	0.080	266.524	3.150	6.753	0.070	18
6.850	0.025	269.674	0.984	6.822	0.025	19
6.875	0.070	270.658	2.740	6.847	0.067	20
6.944	0.150	273.398	5.906	6.917	0.149	21
7.094	0.080	279.304	3.150	7.066	0.090	22
7.174	0.080	282.454	3.150	7.156	0.080	23
7.254	0.080	285.603	3.150	7.236	0.098	24
7.334	0.120	288.753	4.724	7.334	0.120	25
7.454	0.000	293.477	0.000	7.454	0.000	26

TABLE OF DIMENSIONS - FORWARD TORUS (Plug)
Radial Line, Midplane of Octant
Basis:

NI of System= 30 MegAmp-turns

Meters		Inches		Meters(cold)		
r	dr	r	dr	r	dr	
0.780	0.018	30.709	0.709	0.780	0.018	1
0.798	0.050	31.417	1.969	0.798	0.048	2
0.848	0.065	33.386	2.559	0.846	0.065	3
0.913	0.050	35.945	1.969	0.911	0.048	4
0.963	0.199	37.913	7.843	0.959	0.199	5
1.163	0.206	45.787	8.109	1.158	0.206	6
1.370	0.025	53.929	0.980	1.364	0.025	7
1.395	0.050	54.913	1.969	1.389	0.052	8
1.445	0.065	56.882	2.559	1.441	0.065	9
1.510	0.050	59.441	1.969	1.506	0.054	10
1.560	0.025	61.409	0.984	1.560	0.025	11
1.585	0.131	62.394	5.141	1.585	0.131	12
1.715	0.322	67.534	12.672	1.715	0.322	13
2.037	0.168	80.207	6.608	2.037	0.168	14
2.205	0.040	86.815	1.575	2.205	0.040	15
2.245	0.050	88.390	1.969	2.245	0.044	16
2.295	0.065	90.358	2.559	2.289	0.065	17
2.360	0.050	92.917	1.969	2.354	0.046	18
2.410	0.025	94.886	0.980	2.400	0.025	19
2.435	0.103	95.870	4.074	2.425	0.103	20
2.539	0.149	99.961	5.882	2.529	0.149	21
2.689	0.050	105.866	1.969	2.678	0.054	22
2.739	0.065	107.835	2.559	2.732	0.065	23
2.804	0.050	110.394	1.969	2.797	0.057	24
2.854	0.047	112.362	1.850	2.854	0.047	25
2.901	0.000	114.213	0.000	2.901	0.000	26

large Forward Torus (End Cap)

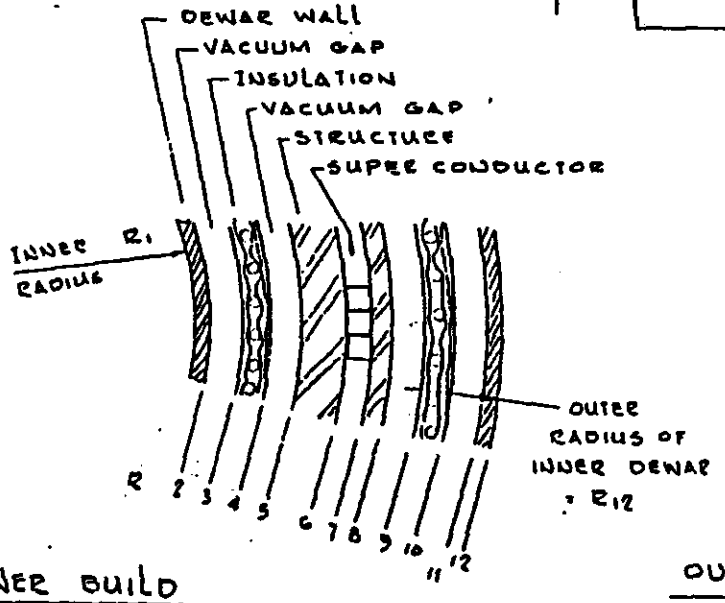

INNER BUILD

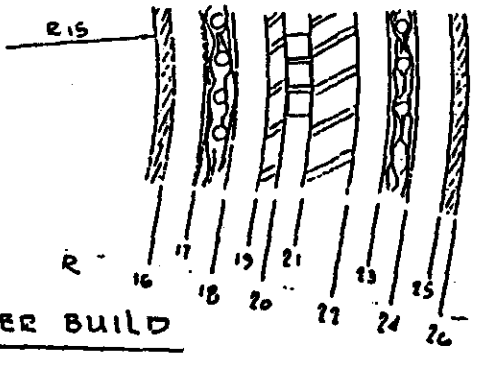

OUTER BUILD

Table 7. Summary Characteristics and Results for Detector Toroids

	Central Torus	
Total Ampere-turns	MAt	30.08
Field-Radius product	T-m	6.016
Nominal Bending Length	T-m	4 @ 90°
Dewar Inner Radius	m	3.00
Dewar Outer Radius	m	7.46
Length	m	21.0
Stored Energy (shell)	GJ	1.29
Toroid Inductance	H	1.61
Axial Separating Force	m tons	7590
Centering Force/Octant	m tons	4020
Conductor Current	kA	40
Conductor Conduit Square	mm	33.3
Turn Length (nom. rect.)	m	49
Number of Turns		752
Conductor Length	km	36.8
Coil Radii		
Centerline Inner	m	3.495
Centerline Outer	m	6.911
Surface Inner Cyl.	m	3.460
Surface Outer Cyl.	m	6.876
Peak Surface Field	T	1.91
Coil Cavity Current Density	kA/sq.cm.	2.9
Turns/Layer/Octant		47
Number of Layers		2
Angle Subtended, conductor	deg	0.5514
Angle Subtended, coil cav.	deg	30.528
Angle Available, local suppt.	deg	4.611
Corresponding arc length	m	0.2784
Angle Subtended, oct.struct.	deg	38.160
Angle Subtended, oct.joint	deg	6.84
Warm Access Manhole Size	inches	20 x 27
Structure Thicknesses:		
Inner Cylinder	m	0.20
Outer Cylinder	m	0.15
Inner Cyl. Joint	m	0.40
Outer Cyl. Joint	m	0.30
Planar End Face	m	0.15

Table 7. Summary Characteristics and Results for Detector Toroids (contd)

	Central Torus	
NASTRAN Element Stresses:		
Hoop Stress at z=0		
Inner Cyl.	ksi	-3.0
Outer Cyl.	ksi	+2.0
Cyl. Bending Stress		
Inner	ksi	-5.4
Outer	ksi	+6.1
Max. Bending Stress		
at Inner Corner		
@ centerline of joint	ksi	+23.0
@ centerline of oct.	ksi	+25.2
Radial Displacements:		
Inner Cyl.,octant center	mm	-1.1
Outer Cyl.,octant center	mm	-3.1
Axial Displacement:		
Maximum, at end face ctr.	mm	+/-17.0
Stress Concentration due to manhole		
k membrane		2.8
k fiber stress		2.5

Note:

For the shorter central torus used with the end cap configuration the nominal length is 15 m and the stress values are nearly identical to those listed above. The axial separating force is the same. The altered parameters are:

Stored Energy	GJ	0.92
Inductance	H	1.15
Centering Force/Octant	m tons	2870

Forward Torus (Plug Type)

Total Ampere-turns	MAt	30.72
Field-Radius product	T-m	6.144
Nominal Bending Length	T-m	10.5 @ 10°
Dewar Inner Radius	m	0.78
Dewar Outer Radius	m	2.90
Length(magnetic)	m	3.00
Stored Energy (shell)	GJ	0.18
Toroid Inductance	H	0.23
Axial Separating Force	m tons	7490
Centering Force/Octant	m tons	1550

Table 7. Summary Characteristics and Results for Detector Toroids (contd)

Forward Torus (Plug Type)		
Conductor Current	kA	40
Conductor Conduit Square	mm	33.3
Turn Length (nom. rect.)	m	8.6
Number of Turns		768
Conductor Length	km	6.6
Coil Radii		
Centerline Inner	m	1.266
Centerline Outer	m	2.486
Surface Inner Cyl.	m	1.163
Surface Outer Cyl.	m	2.434
Peak Surface Field	T	5.89
Coil Cavity Current Density	kA/sq.cm.	2.7
Turns/Layer/Octant		16
Number of Layers		6
Angle Subtended, conductor	deg	1.640
Angle Subtended, coil cav.	deg	31.187
Angle Available, local suppt.	deg	4.940
Corresponding arc length	m	0.100
Angle Subtended, oct.struct.	deg	38.984
Angle Subtended, oct.joint	deg	6.00
Warm Access Manhole Size	inches	10 x 18
Structure Thicknesses:		
Inner Cylinder	m	0.20
Outer Cylinder	m	0.15
Inner Cyl. Joint	m	0.30
Outer Cyl. Joint	m	0.30
Planar End Face	m	0.15
NASTRAN Element Stresses:		
Hoop Stress at z=0		
Inner Cyl.	ksi	-8.2
Outer Cyl.	ksi	+5.2
Cyl. Bending Stress		
Inner	ksi	+8.9
Outer	ksi	+9.4
Max. Bending Stress		
at Inner Corner		
@ centerline of joint	ksi	+38.1
@ centerline of oct.	ksi	+36.3

Table 7. Summary Characteristics and Results for Detector Toroids (contd)

	Forward Torus (Plug Type)	
Radial Displacements:		
Inner Cyl.,octant center	mm	-0.95
Outer Cyl.,octant center	mm	+1.33
Axial Displacement:		
Maximum, at end face ctr.	mm	5.0
	Forward Torus (End-Cap Type)	
Total Ampere-turns	MAt	30.72
Dewar Inner Radius	m	0.78
Dewar Outer Radius	m	7.46
Stored Energy (shell)	GJ	0.47
Axial Separating Force	m tons	19500
Centering Force/Octant	m tons	2665
Structure Thicknesses:		
Inner Cylinder	m	0.20
Outer Cylinder	m	0.15
Inner Cyl. Joint	m	0.30
Outer Cyl. Joint	m	0.30
Planar End Face	m	0.30
NASTRAN Element Stresses:		
Hoop Stress at z=0		
Inner Cyl.	ksi	8.4
Outer Cyl.	ksi	
Cyl. Bending Stress		
Inner	ksi	10.43
Outer	ksi	
Max. Bending Stress at Inner Corner		
@ centerline of joint	ksi	86.6*
@ centerline of oct.	ksi	98.7*
Radial Displacements:		
Inner Cyl.,octant center	mm	-1.17
Outer Cyl.,between octants	mm	-4.97
Axial Displacement:		
Maximum, at end face ctr.	mm	+/-37.8

Note: Asterisk (*) indicates value above allowed limit.

The highest stress in a toroid is usually at the inner corner. For the three configurations examined, all with sharp corners, this peak stress exceeds allowed limits for the end cap torus alone. The end face thickness chosen for this model is in fact, too thick, and overbends the inner cylinder. This stress can easily be reduced by the addition of tie plates in azimuthal planes which interconnect the end faces. The axial separating force is then reacted by tension in the plate as well as the parallel path through the annular disk and cylinders. The load and moment which pass through the corner can be reduced substantially by using this additional structure.

A more complete description of the finite-element model and results is provided in an appendix.

The objective here was the demonstration of feasibility. The initial estimates of needed thickness were chosen to produce a feasible result in the first analysis. This has been done. There is however, considerable room for improvement.

The results in Table 7 can be compared with the short summary of material properties listed in Table 8 below.

Table 8. Properties of the Structural Aluminum

Alloy: Aluminum 2219-T87
Form: Plate, over 2" thick
Specification: MIL-A-8920A, ASTM B209

Property		Testing Temperature (K) 297	20
Elastic Modulus,Min.,Mpsi			
Longitudinal		10.2	10.6
Transverse		10.7	9.4
Poissons Ratio		0.33	0.318
Thermal Expansion; RT to 4K		-0.396%	
Density (gms/cu.cm.),(m tons/cu.m.)		2.85	
Ultimate Tensile Strength (ksi)			
Longitudinal	Avg.	68.5	98.1
	Min.	66.0	83.6
Transverse	Avg.	68.1	96.3
	Min.	64.3	86.3

Table 8. Properties of the Structural Aluminum (contd)

Tensile Yield Strength 0.2% (ksi)			
Longitudinal	Avg.	55.6	74.3
	Min.	53.4	71.0
Transverse	Avg.	55.4	71.2
	Min.	53.7	68.8
Elongation, percent, 2 inches.			
Longitudinal	Avg.	9.7	10.4
	Min.	6.3	4.7
Transverse	Avg.	8.3	8.6
	Min.	5.0	4.8
Reduction in Area, percent			
Longitudinal	Avg.	19	15.9
	Min.	15.1	13.4
Transverse	Avg.	13.2	12.5
	Min.	9.6	11.1
Tensile Notch Toughness K_t=10 (ksi)			
Longitudinal	Avg.	66.8	85.0
	Min.	63.9	80.6
Transverse	Avg.	55.7	65.5
	Min.	51.7	63.6
Fracture Toughness K_{Ic}, Min., (ksi,sq.rt.inches)			
Bend Specimens (T-S)		36.2	47.2
Compact Specimens (T-S)		26.1	33.1
Weld Metal, Plate, Pulse TIG Weld, 2319 filler, as welded			
UTS	Min.	38.2	46.4
YS	Min.	18.0	23.3

The materials data suggest that a machined and bolted structure be designed with particular attention to stress risers. Welding, if at all necessary, must be restricted to lower stress areas.

MAGNETIC FIELD SHAPE CONSIDERATIONS

A plot of magnetic flux is shown in Fig. 13. The field in the actual toroid is shown in Fig. 14. Note that the influence of the gap extends beyond its edge. The structural worst-case, i.e., large gaps, is also the magnetically worst (leakiest) case. Further work should reduce the gap size and improve the field confinement. Figure 15 illustrates the field improvement as the gap is reduced. The leakage can also be reduced by adding coil turns on both sides of the gap and/or by

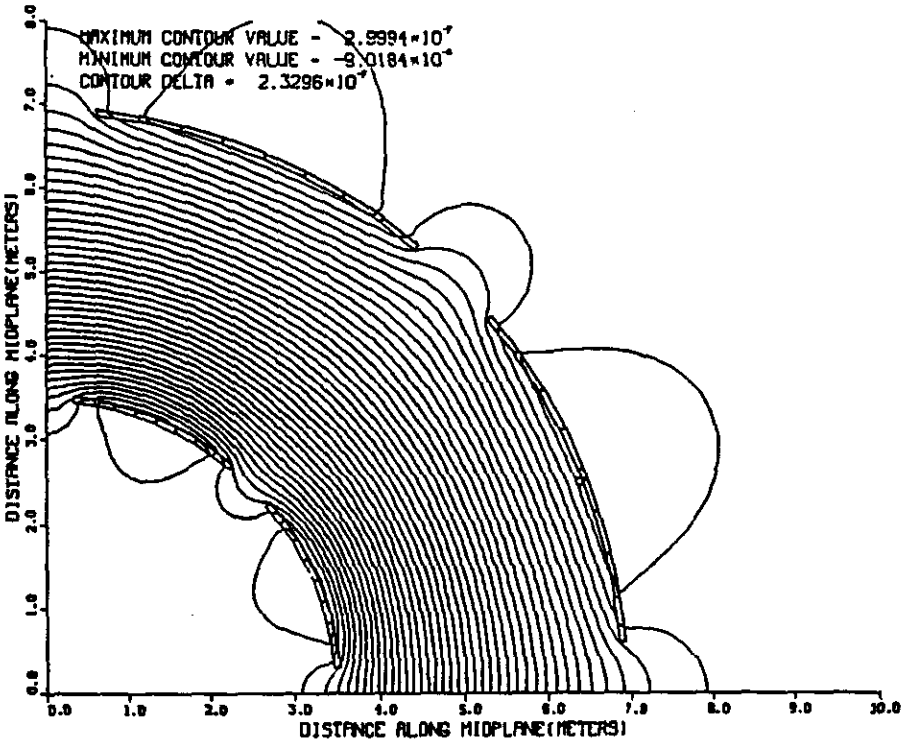

Fig. 13
Magnetic Flux Contours

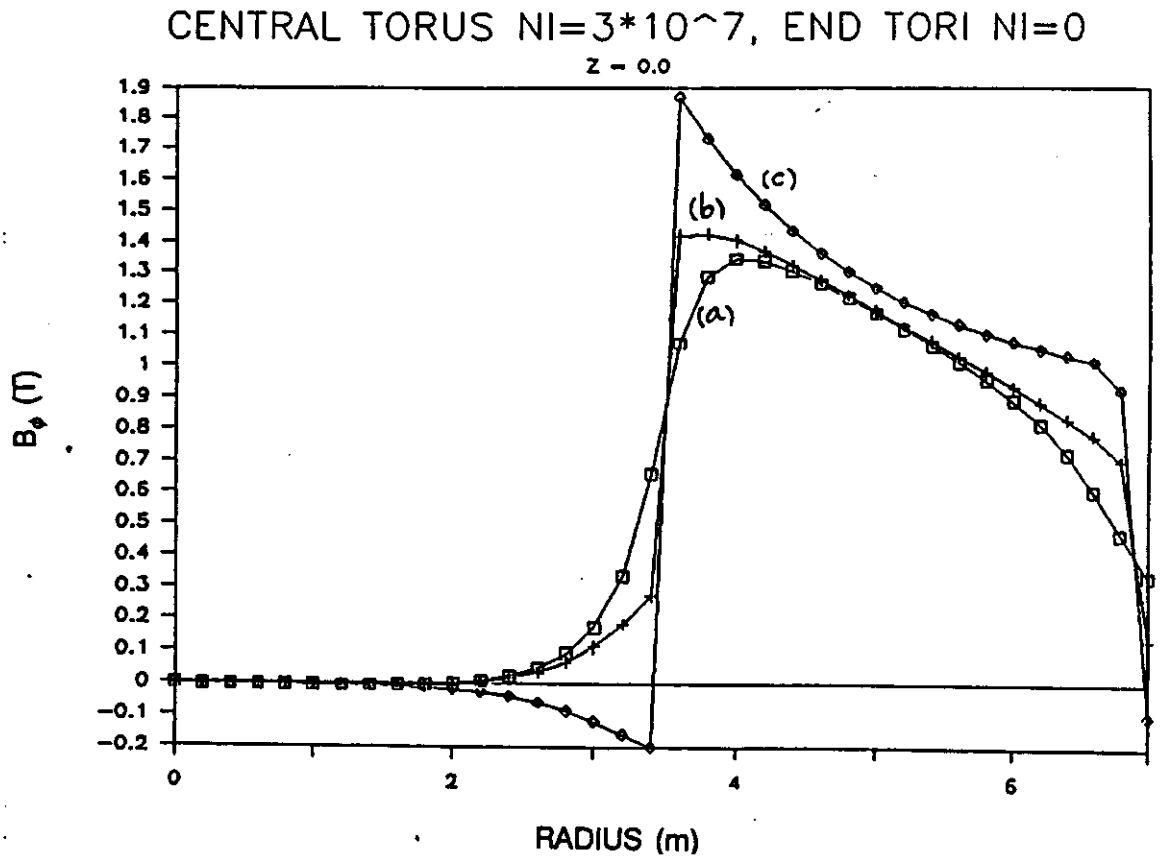

Fig. 14
Field strength vs radius
at z=0 for
(a) = 0.00 deg. (at gap midplane)
(b) = 4.52 deg. (at gap edge)
(c) = 22.5 deg. (at midplane of octant coil)

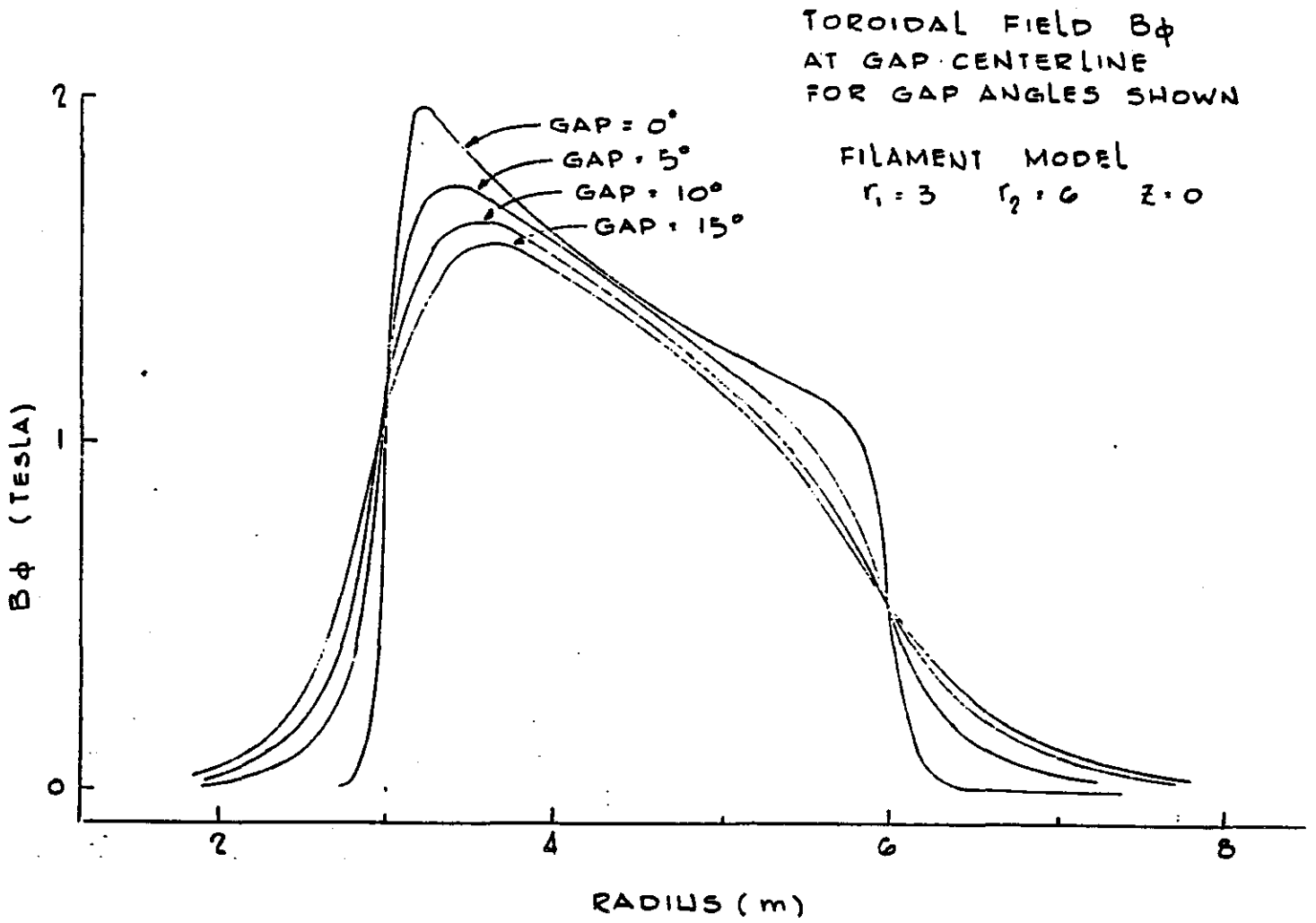

Fig. 15
Field strength at gap centerline
vs. radius
for gap angles of 0, 5, 10, and 15 deg.

placing iron shims between coils. The iron may be incorporated into the octant joints or made part of the dewar shell.

Plots of central toroid stray field at the locations of the windings of the end plug toroid were used to estimate the forces between toroids, since these loads must be carried to a warm support. The results, Table 9, are small, even compared to gravity loads.

Table 9. Estimated Forces on an End Plug torus Due to the Stray Field of the Central Torus

Radial	≈0 (toroid in stable equilibrium with 15 tonnes inward per octant)
Axial	11 tons net, toward the Z= 0 plane
Azimuthal	≈0 (unstable equilibrium)

NOTE: Forces on end cap toroid were not estimated.

ASSEMBLY

We assume it is feasible to fabricate the 24 octants in the factory, complete with structure, coil, and dewar, and ship them to the SSC site. In the hall, an assembly superstructure is envisioned, used only during initial erection and then removed, on which completed octants are stacked. The sequence is symmetric about a vertical plane containing the axis of the toroid and proceeds from the ground on up. The assembly might be on tracks such that a torus could be moved away from the beam line to facilitate detector maintenance. As each octant is positioned, its structural joints to adjacent octants are bolted and locked, the field welds joining the dewars are made, and appendages are attached. A table of weights and component sizes is provided in an appendix.

COMMENTARY

No technically insurmountable problems which would preclude construction of a toroidal detector have been found in this study. It would be the largest superconducting toroid ever built and a major engineering effort requiring a dedicated design and construction team.

This initial concept is necessarily incomplete and a list of engineering tasks for a "next step" is provided below.

1. Evaluate the effects on the structure, the conductor, and fabrication costs, of subdividing the winding cross section azimuthally and treating the end flange, inner cylinder, outer cylinder, and teeth joining them as a hollow plate beam. Initially use three unequally spaced teeth, with the two end cavities being smaller azimuthally than the two central cavities.

2. Evaluate fabrication of the octant structure as a thick inner cylinder with machined winding cavities and a cover cylinder, and also as two rolled cylinders separated by extruded rectangular bars fastened with radial through-bolts.

3. Evaluate the addition of structural plates within the toroidal field volume. Initially, one per octant in an azimuthal plane connected to the cylinders and end faces.

4. Establish the minimum size and the locations of all warm access openings.

5. Evaluate arrangements for reducing the difference between the warm gaps and the gaps between windings.

6. Perform a buckling analysis of the modified structural model.

7. Analyze the structure during the intermediate stages of assembly.

8. Perform a formal fault analysis.

9. Design an octant joint in more detail.

10. Analyze the dewar structure using FEM.

11. Evaluate forces between toroids, conceptualize a support structure to grade.

12. Evaluate conductor-in-conduit construction with reduced bend radius.

13. Make a Preliminary Design of a coil lead arrangement.

REFERENCES

1. "The Pure Tension Shape of a Thick Torus," D. W. Weissenburger, U. R. Christensen, J. Bialek; Princeton Plasma Physics Report PPPL-1353, July 1977.

2. U.S.Patent 3,736,439; "Moment-Free Toroidal Magnet Design," J. File, R. G. Mills, G. V. Sheffield and P. Bonanos; May 29, 1973.

3. "Bow-Shaped Toroidal Field Coils," P. Bonanos; Princeton Plasma Physics Report PPPL-1790, May 1981.

4. "Optimal Shape of a Toroidal Solenoid," V. D. Shfranov; *Soviet Physics-Technical Physics* Vol. 17, No. 9, March, 1973. Translated from *Zhurnal Tekhnicheskoi Fiziki* Vol. 42, Nr. 9.

5. "The IEA Large Coil Task; Development of Superconducting Toroidal Field Magnets for Fusion Power," ed. by D. S. Beard et al; compiled by P. N. Haubenreich et al.; *Fusion Engineering and Design* Vol. 7(1&2), 1988.

6. "Internal Pressure Effects in the Airco-LCT Conductor Sheath," J. N. Luton, J. A. Clinard, J. W. Lue, and W. H. Gray; *Proceedings of the 9th International Conference on Magnet Technology*, Zurich, Switzerland, September 9-13, 1985.

7. "Rational Design of High-Current Cable-in-Conduit Superconductors," L. Dresner; presented at the IAEA Specialists' Meeting on Superconducting Magnets and Materials, Tokyo, Japan, September 4-6, 1989.

8. "High-Field, High-Current-Density, Stable Superconducting Magnets for Fusion Machines," J. W. Lue, L. Dresner, and M. S. Lubell; *[Proceedings] 7th International Workshop on Stellarators*, Oak Ridge, Tennessee, April 10-14, 1989 (IAEA Technical Committee Meeting).

9. "A Study of Eddy-Current Effects in the Structure of the Westinghouse LCT Coil," J. N. Luton et al.; *IEEE Trans. Magn.* MAG-23:1497-1500, 1987.

ACKNOWLEDGEMENTS

Thanks are given to I. Zatz of PPPL for steering P.B. through the maze of NASTRAN manuals, to M. Pelovitz of PPPL for his flux contour plot, to B. Nelson of ORNL for the field plots and B. Pope of MSU for the plot showing the effect of gap angle.

The text was typed by Sandra Vaughan of ORNL and P.B.

Appendix A

Toroidal Coil Mechanics

SSC · TOROIDAL DETECTOR MECHANICS

FORCES : FOR DISCRETE COILS, CLOSELY SPACED

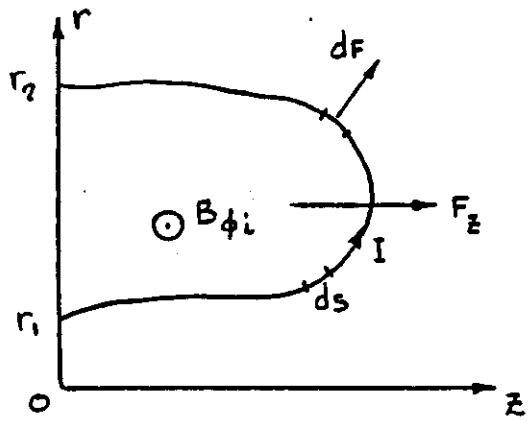

$$d\bar{F} = I\, d\bar{s} \times \bar{B}_{\phi\, AVG}$$

TOROIDAL SHELL APPROXIMATION

$$\oint H_i\, dl = nI \qquad B_{\phi_i} = \mu_0 H_i$$

$$B_{\phi_i} = -\frac{\mu_0 n I}{2\pi r}$$

AXIAL FORCE : F_z

$$F_z = \int_C d\bar{F} \cdot \bar{z} = \int_C (I\, d\bar{s} \times \bar{B}_{\phi_{AVG}}) \cdot \bar{z} = \int_C I\, d\bar{s} \cdot (\bar{B}_{\phi_{AVG}} \times \bar{z})$$

$$\bar{B}_{\phi_{AVG}} \times \bar{z} = B(r)\, \bar{\phi} \times \bar{z} = B(r)\, \bar{r}$$

$$\nabla \times B(r)\, \bar{r} = 0$$

$\therefore$ F_z IS INDEPENDENT OF PATH

RADIAL FORCE : F_r

$$F_r = \int_C d\bar{F} \cdot \bar{r} = \int_C I\, d\bar{s} \cdot (B(r)\, \bar{z})$$

$$\nabla \times B(r)\, \bar{z} = -\frac{\partial B(r)}{\partial r}\, \bar{\phi} \neq 0$$

$\therefore$ F_r SHAPE DEPENDENT, RADIALLY INWARD

TOTAL AXIAL FORCE ON COMPLETE TOROID

$$F_{z_T} = \int_A \frac{B_\phi^2}{2\mu_0}\, dA = \frac{\pi}{\mu_0} (B_{\phi_0} r_0) \ln \frac{r_2}{r_1} = \frac{\mu_0}{4\pi} (nI)^2 \ln \frac{r_2}{r_1}$$

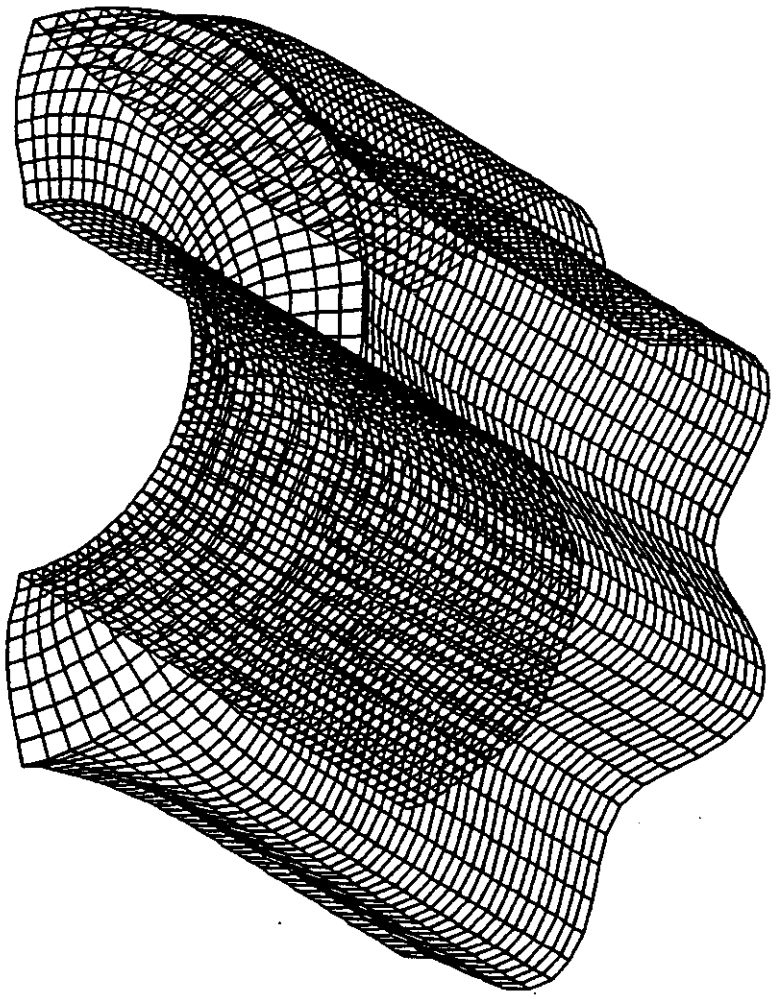

Appendix B

NASTRAN Model and Results

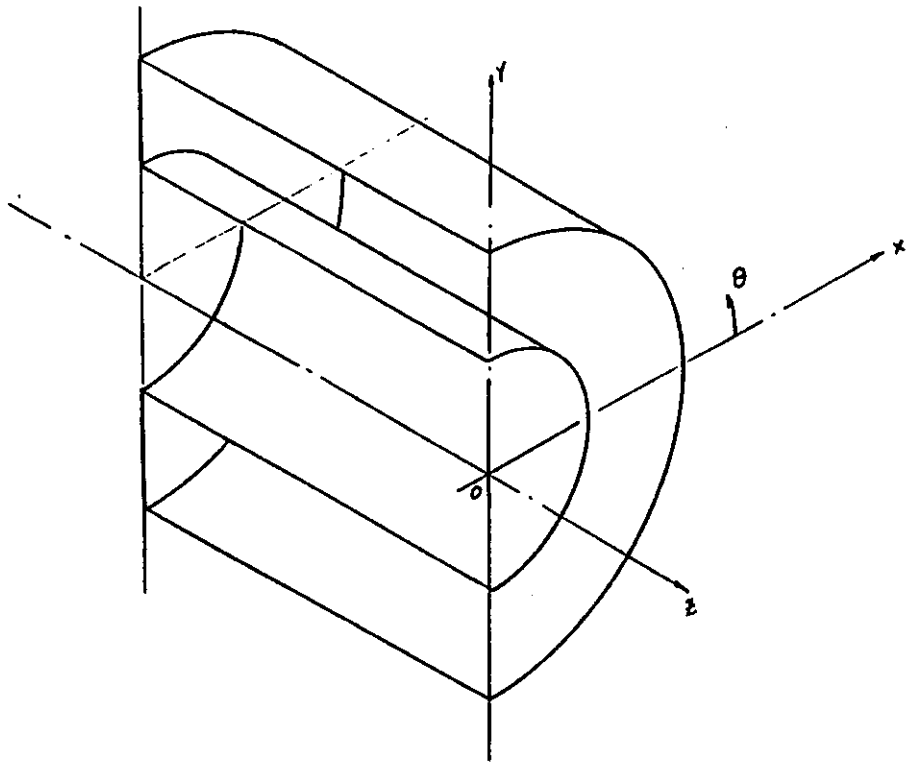

COORDINATE SYSTEMS : INPUT ; RECT. CARTESIAN
OUTPUT ; CYLINDRICAL (DISP.)

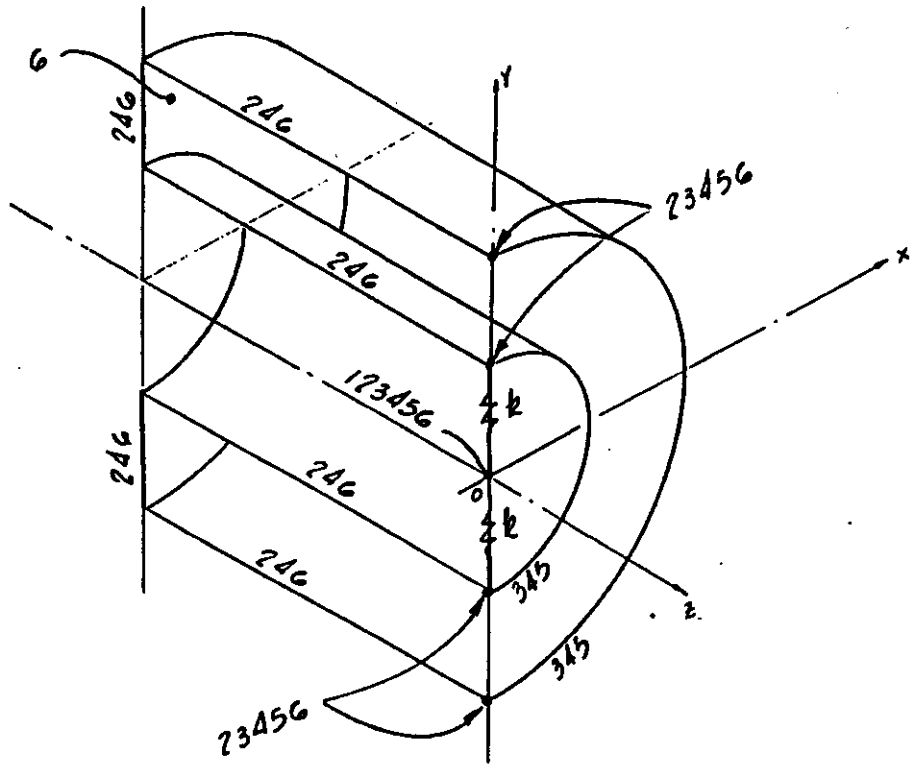

BOUNDARY CONDITIONS : 1 R 4 θ_r
2 θ 5 θ_o

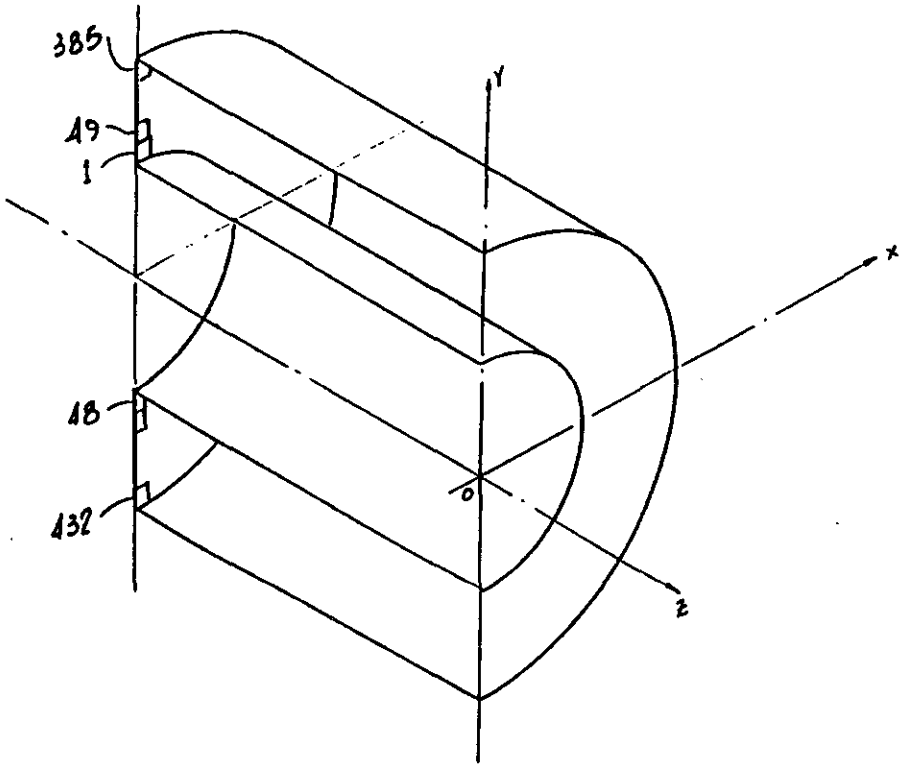

ELEMENT NUMBERING : END FACE (ALL MODELS)

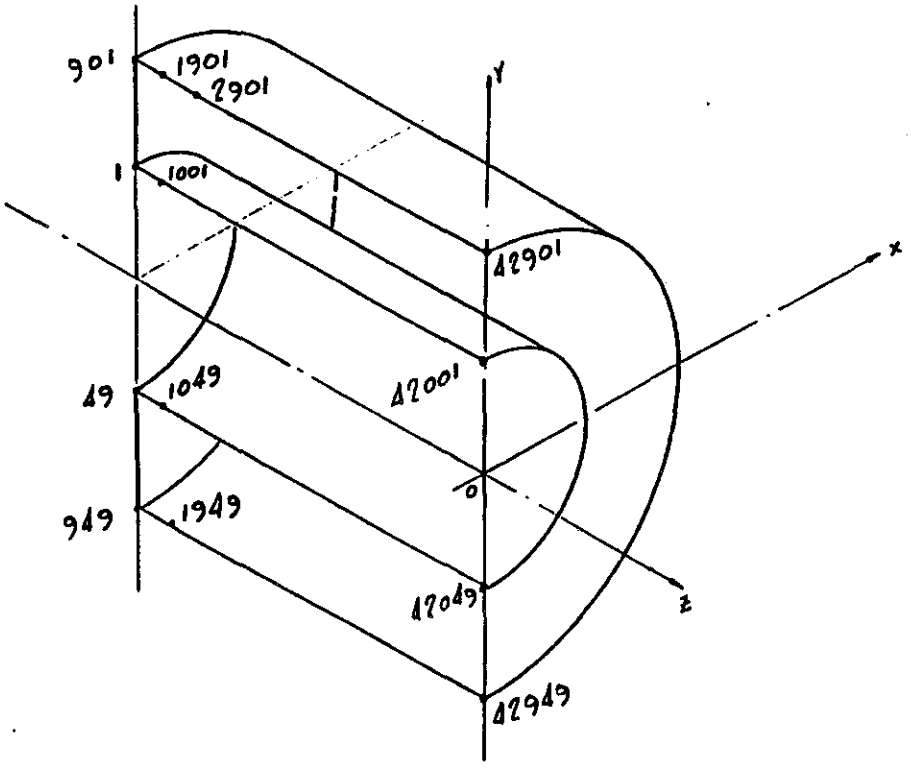

NODE NUMBERING : LONG CENTRAL TORUS

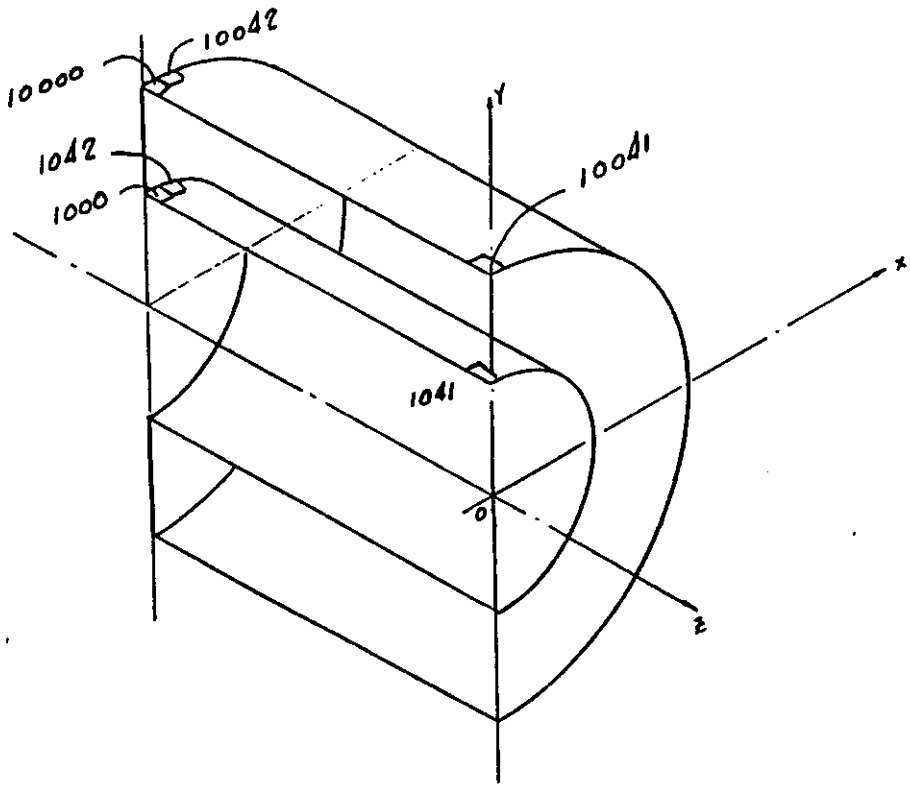

ELEMENT NUMBERING: LONG CENTRAL TORUS

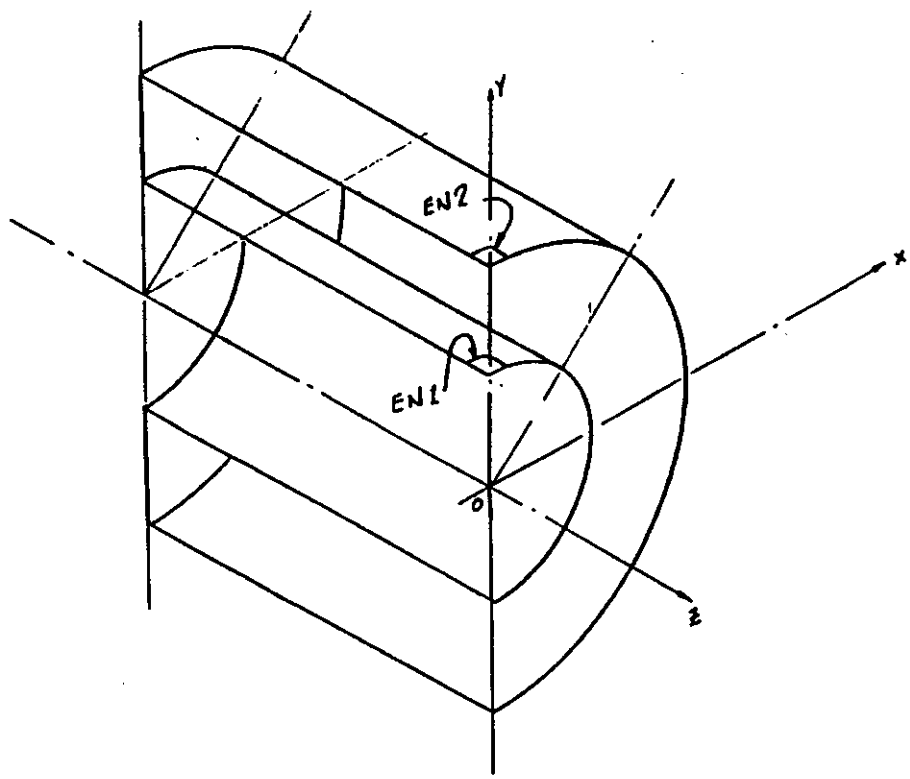

ELEMENT NUMBERING:	EN1	EN2
FORWARD TORII (PLUG OR CAP)	1009	10009
SHORTER CENTRAL TORUS	1029	10029

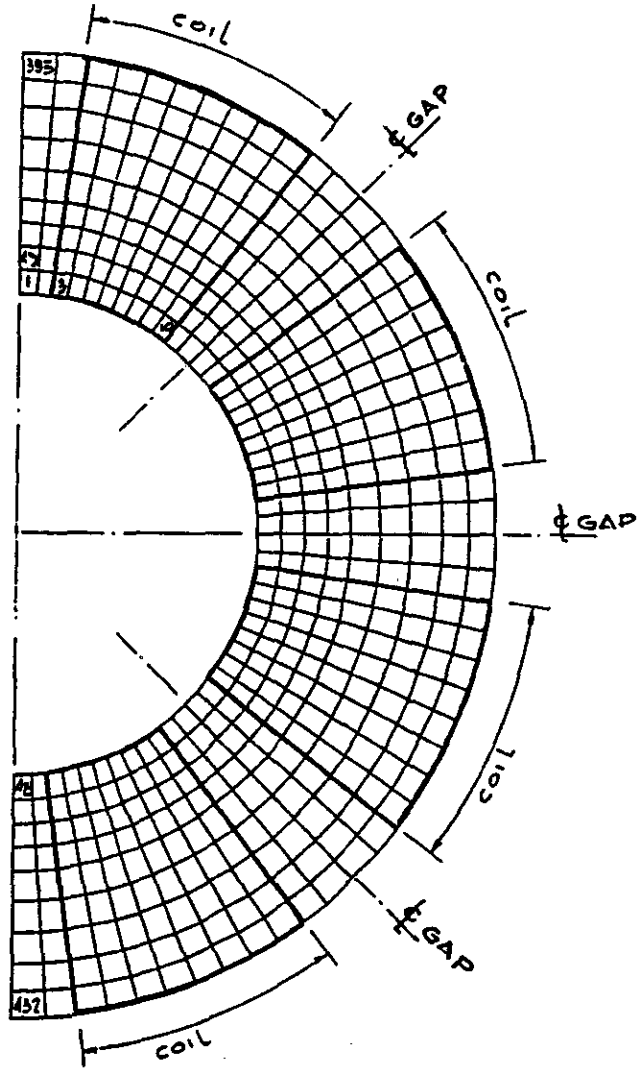

TOROID END FACE

SHOWING
COIL AND GAP
PROPORTIONS

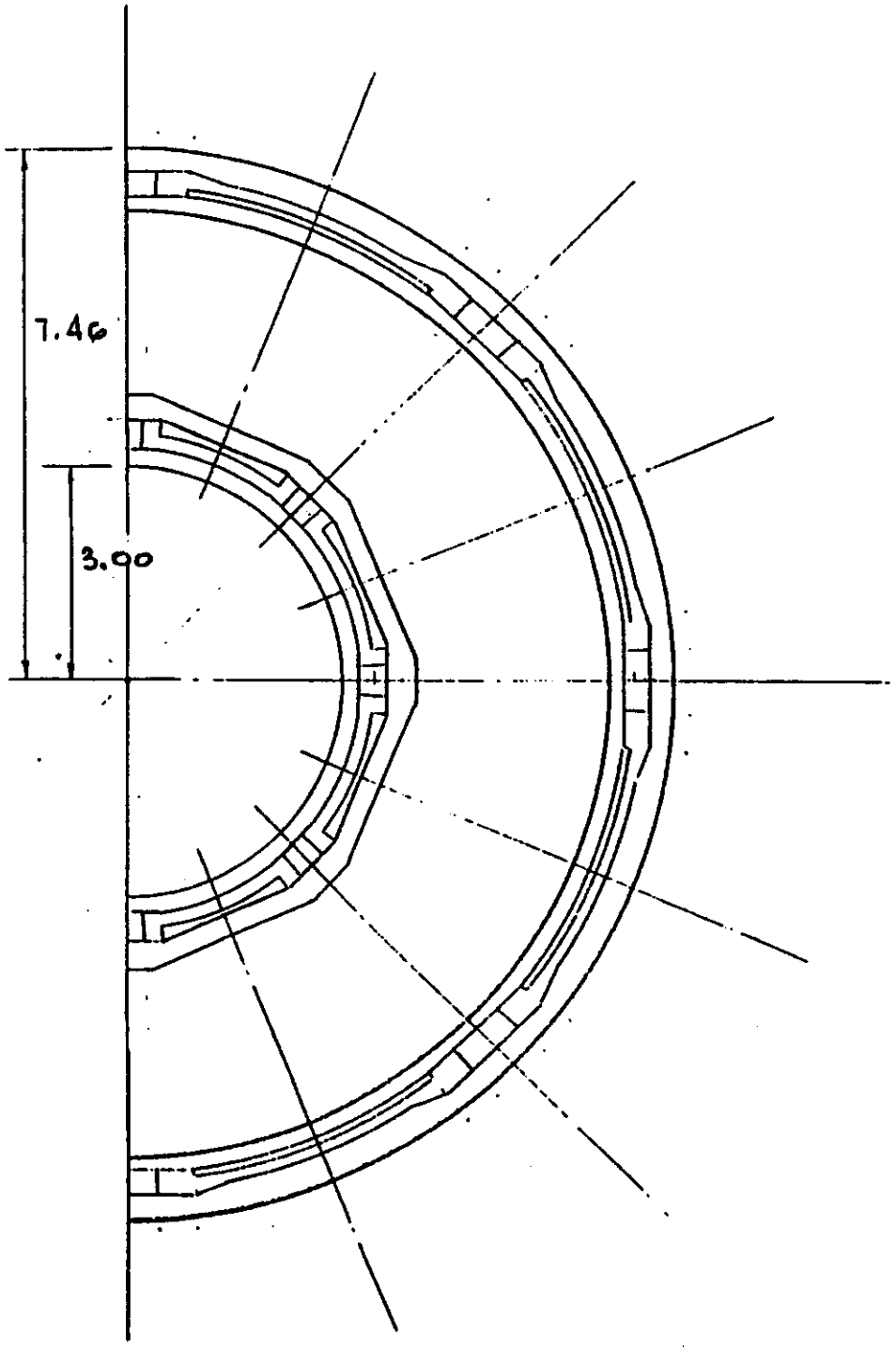

CENTRAL TORUS

CROSS SECTION

PB
7-26-89

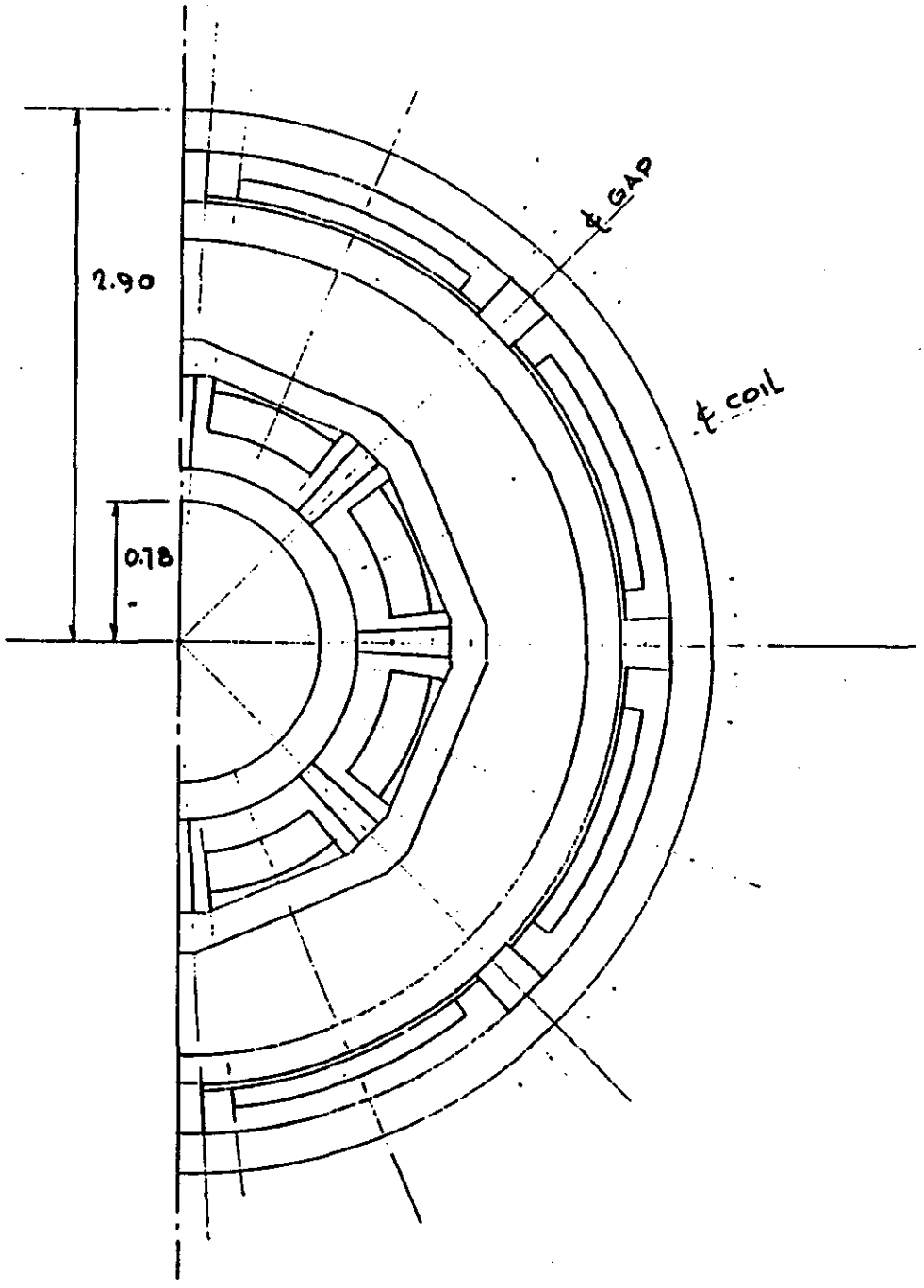

FORWARD TORUS (PLUG)

CROSS SECTION

PB
8·3·89

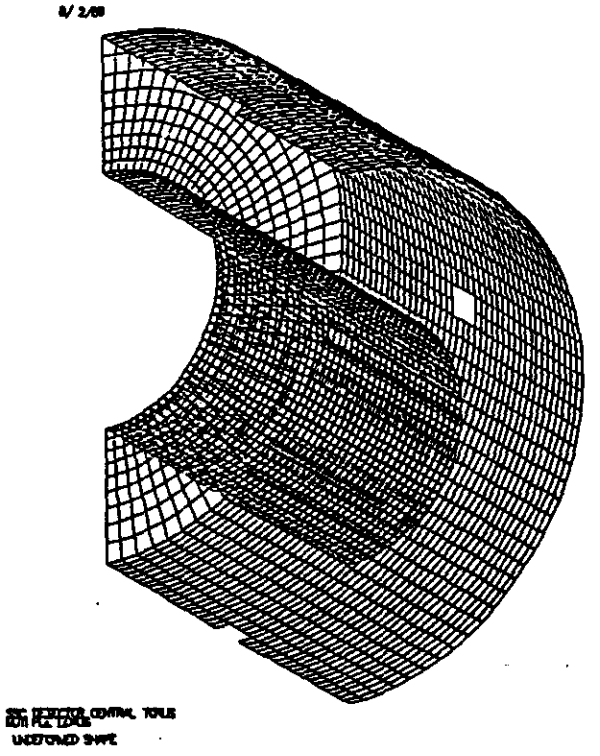

UNDEFORMED SHAPE

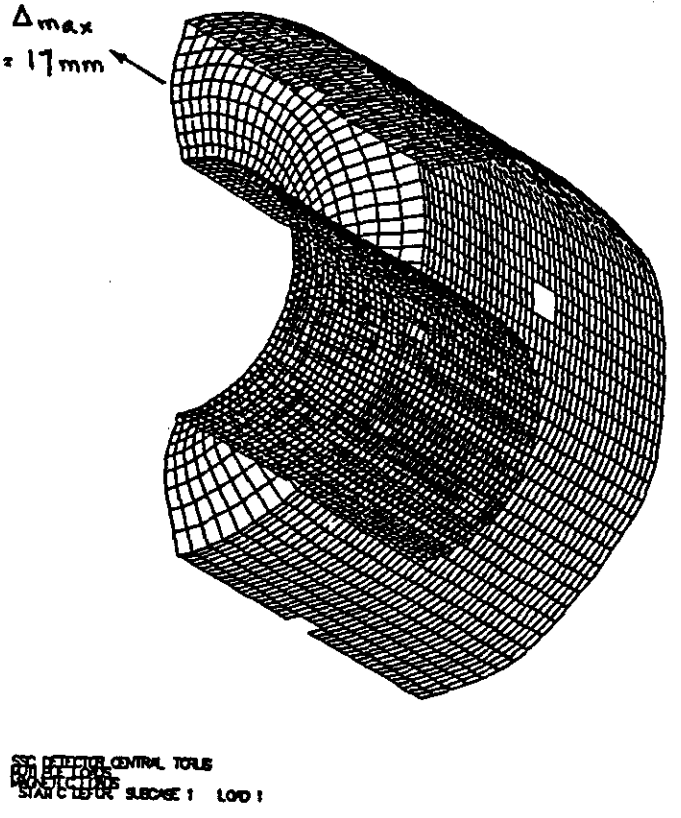

DISTORTION UNDER LOAD

CENTRAL TORUS WITH MANHOLES

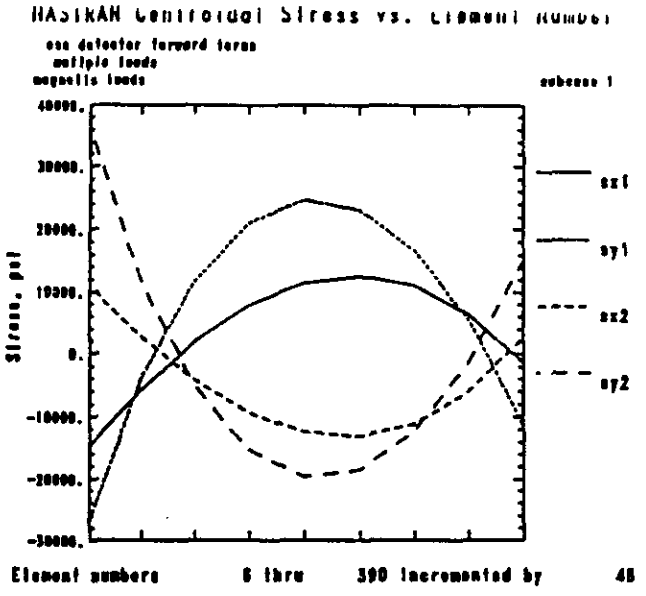

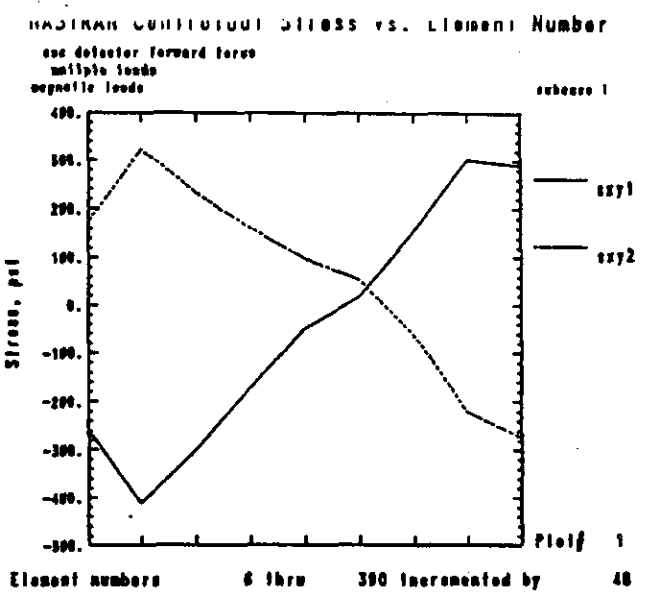

RADIAL STRIP - END FACE @ ℄ COIL

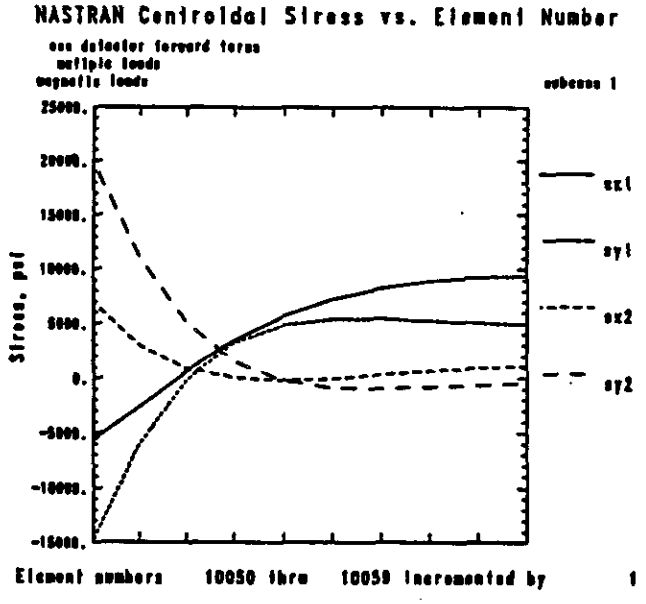

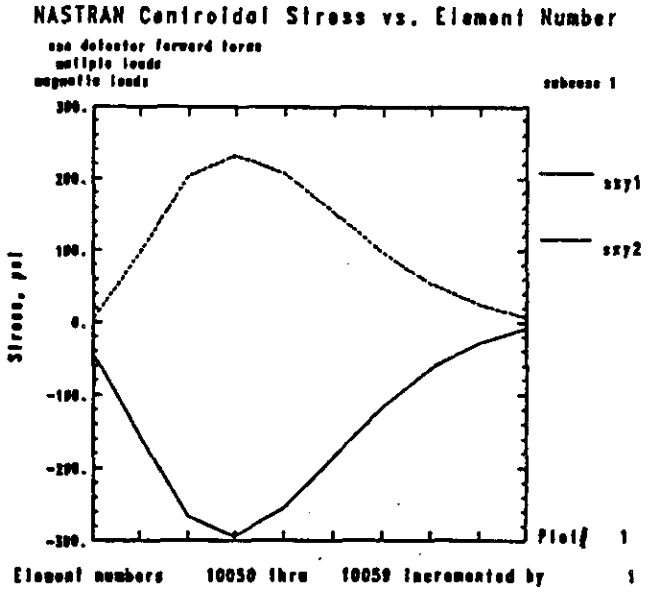

AXIAL STRIP - OUTER CYLINDER @ ℄ COIL

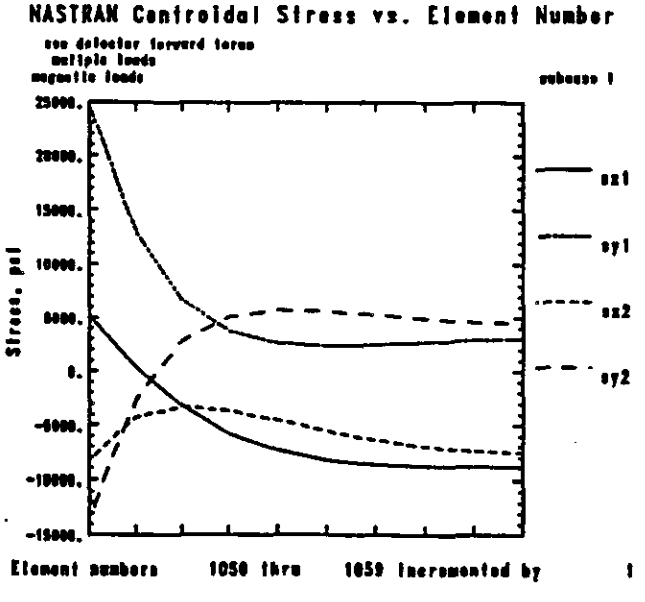

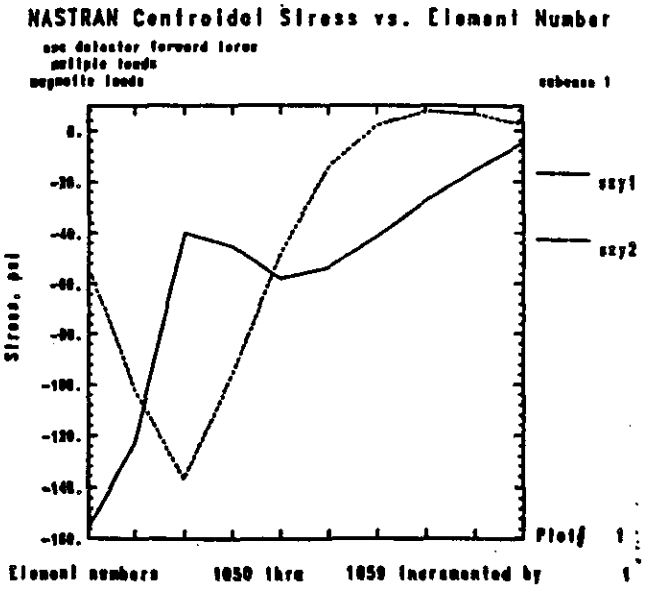

AXIAL STRIP - INNER CYLINDER @ ℄ COIL

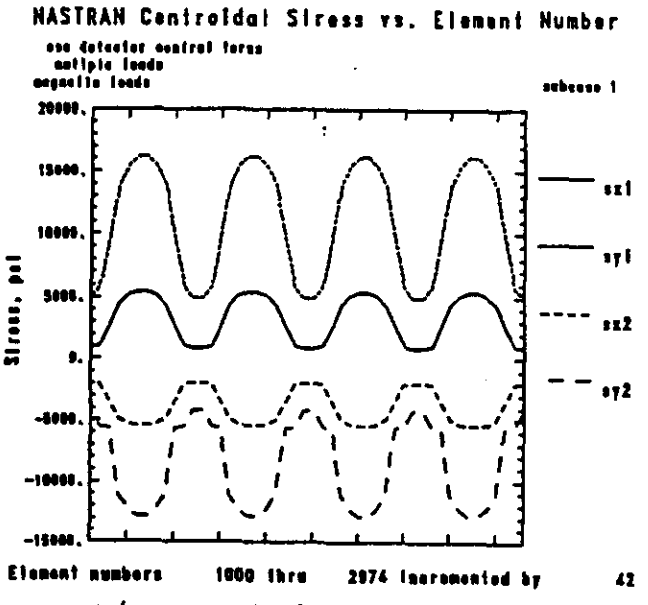

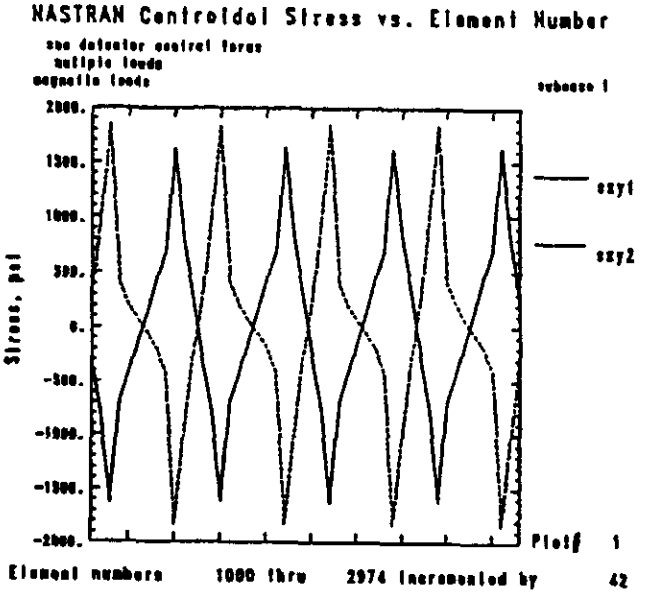

INNER CYLINDER - GIRTH STRIP @ END FACE

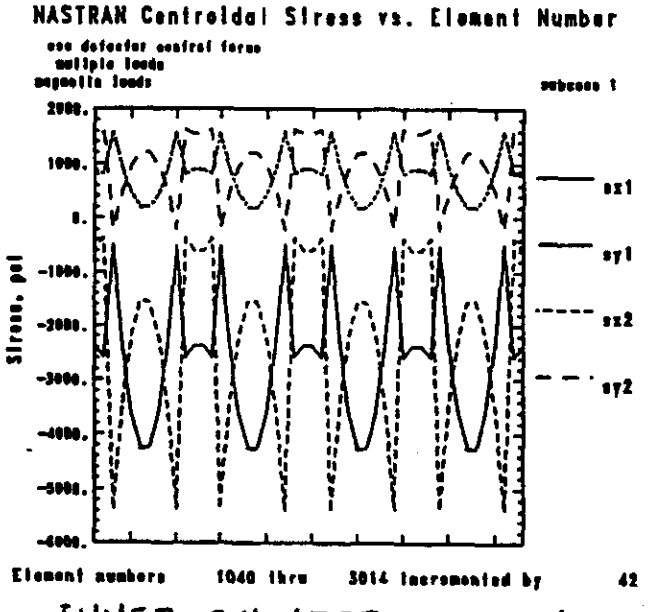

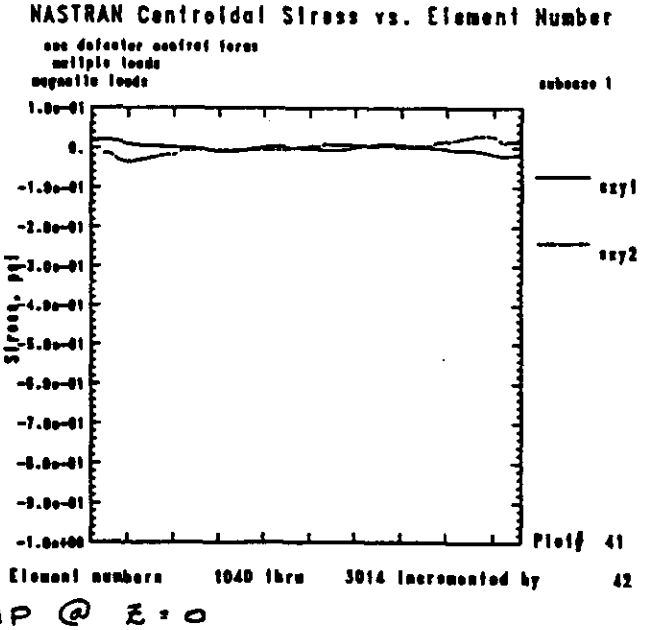

INNER CYLINDER - GIRTH STRIP @ Z = 0

CENTRAL TORUS

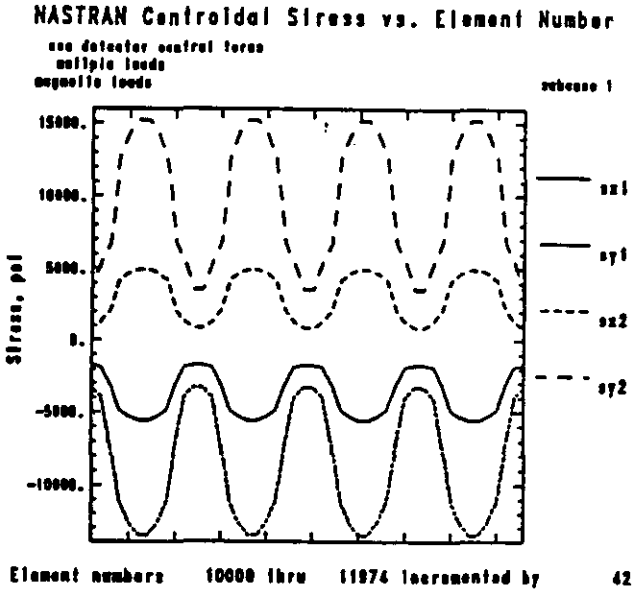

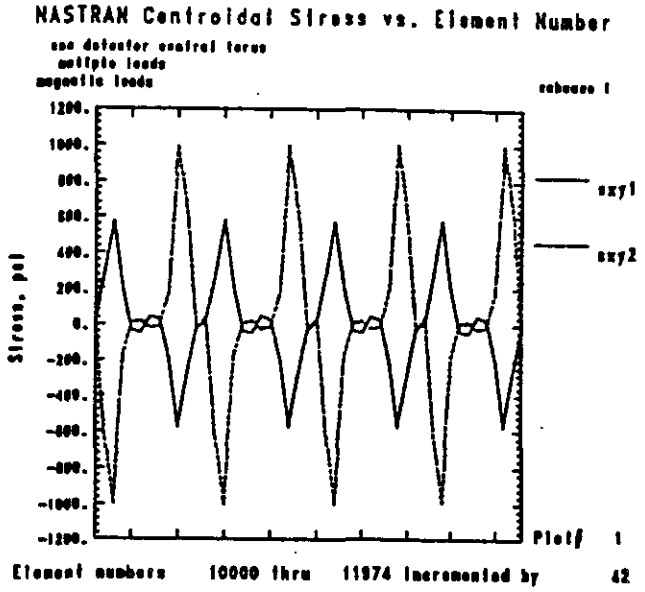

OUTER CYLINDER - GIRTH STRIP @ END FACE

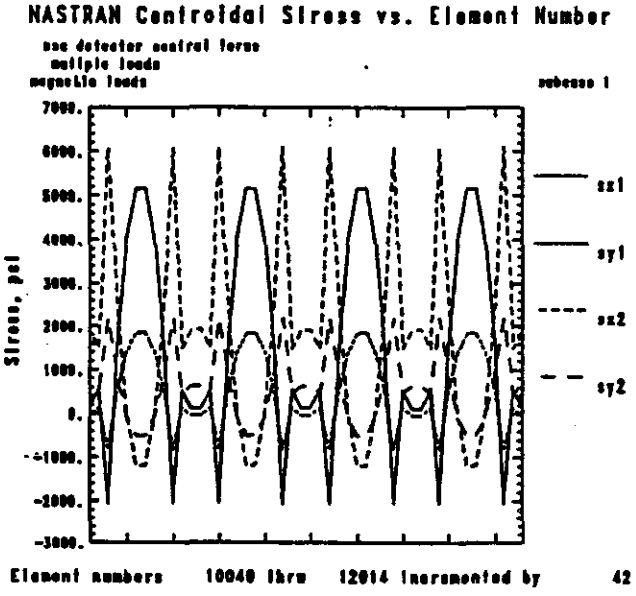

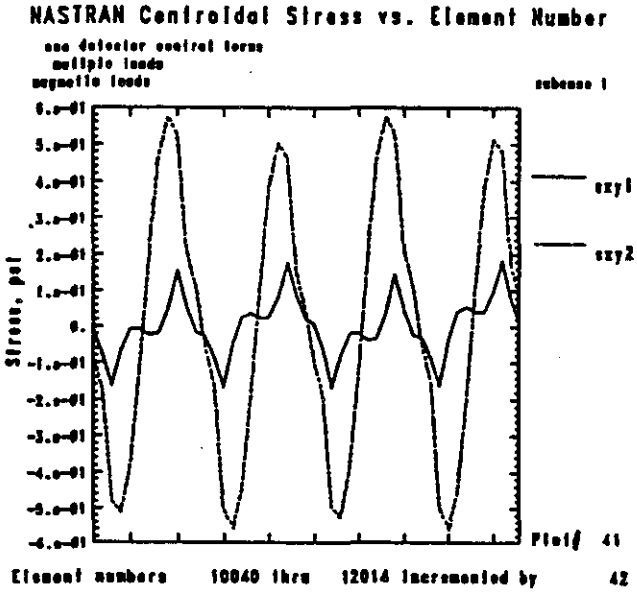

OUTER CYLINDER - GIRTH STRIP @ $z = 0$

CENTRAL TORUS

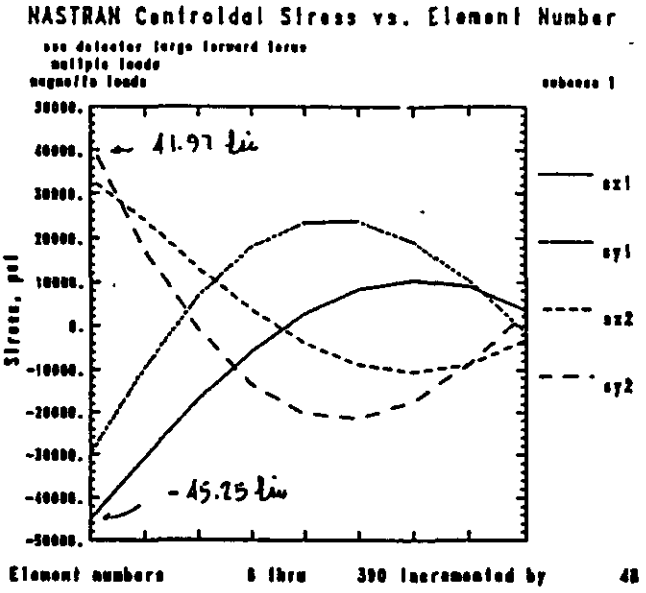

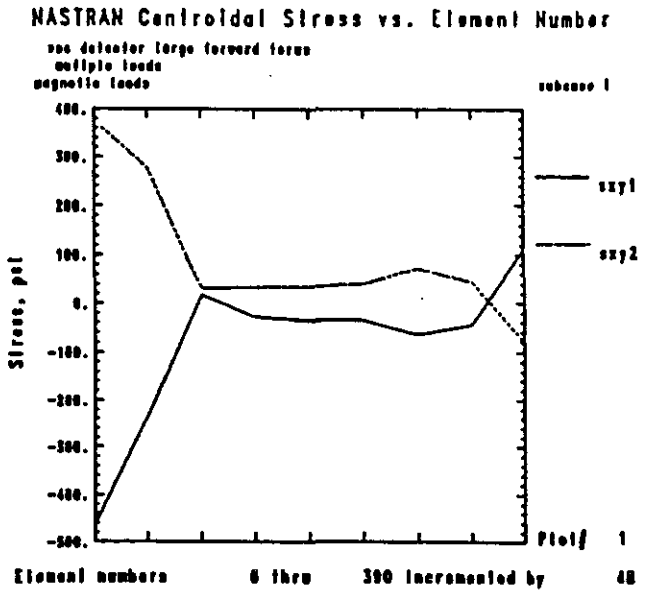

END FACE · RADIAL STRIP AT ℄ COIL

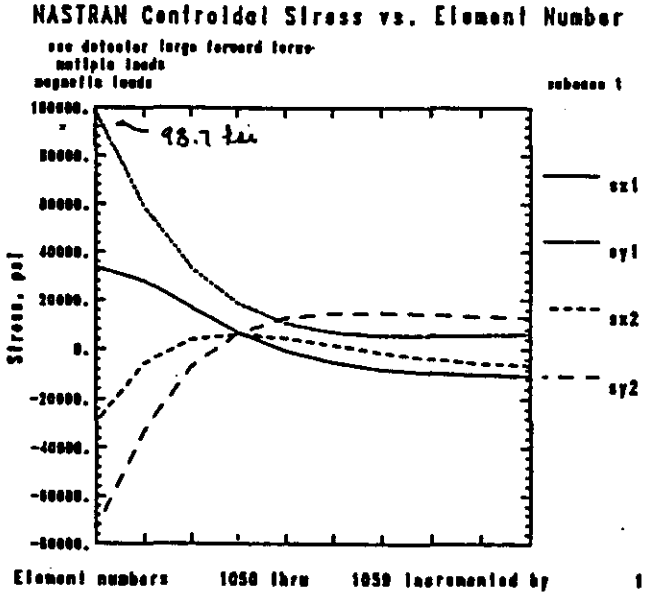

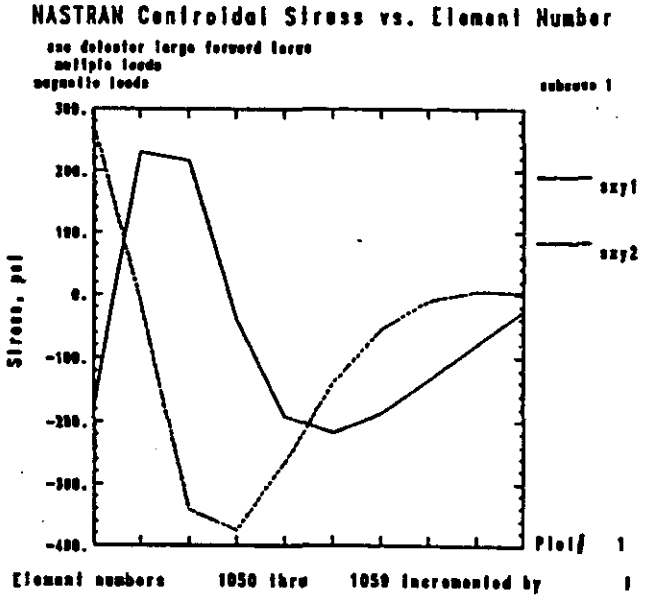

INNER CYLINDER - AXIAL STRIP AT ℄ COIL

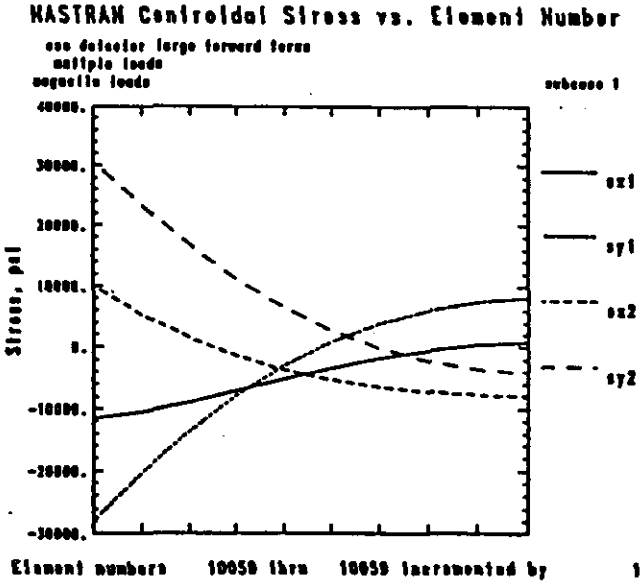

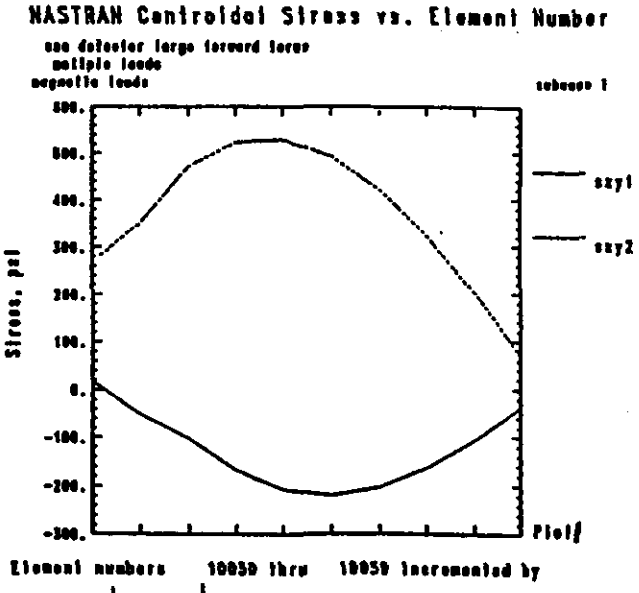

OUTER CYLINDER · AXIAL STRIP AT ℄ COIL

1 7/27/89

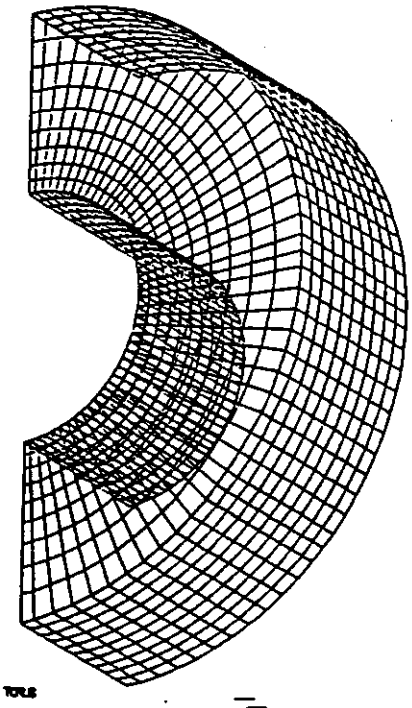

SSC DETECTOR FORWARD TORUS
NON PLUG LOADS
UNDEFORMED SHAPE

UNDEFORMED SHAPE

2 7/27/89 MAX-DEF. = 0.00500545

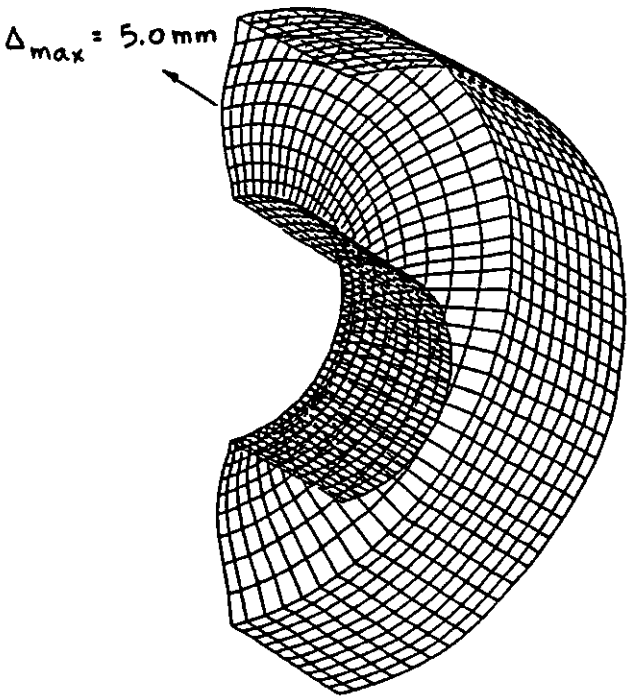

SSC DETECTOR FORWARD TORUS
PLUG LOADS
MAGNIFICATION
STATIC DEFOR. SUBCASE 1 LOAD 1

DISTORTION UNDER LOAD

FORWARD TORUS (PLUG)

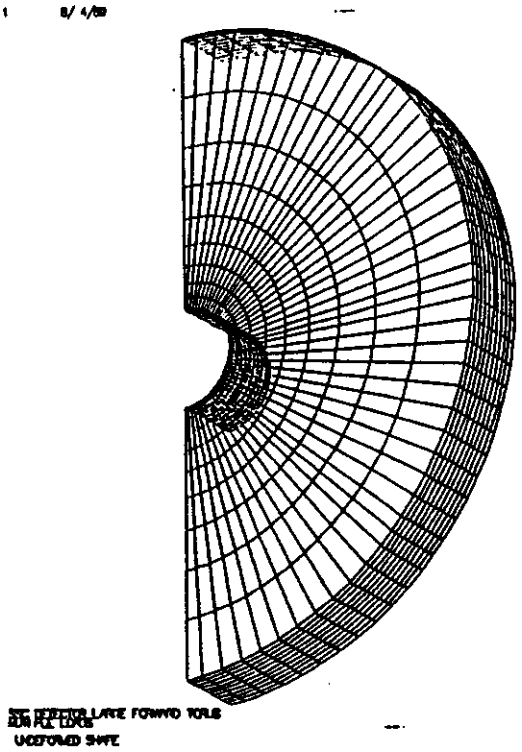

UNDEFORMED SHAPE

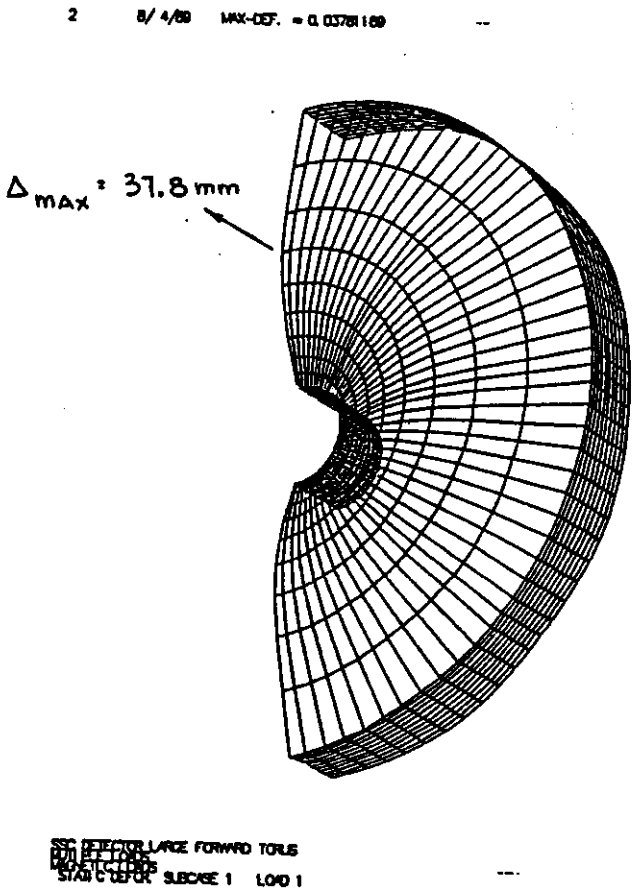

DISTORTION UNDER LOAD

LARGE FORWARD TORUS (END CAP)

Appendix C

Magnetic Field Plots

CENTRAL TORUS NI=3*10^7, END TORI NI=0

ϕ – 22.5, WINDING CENTERLINE

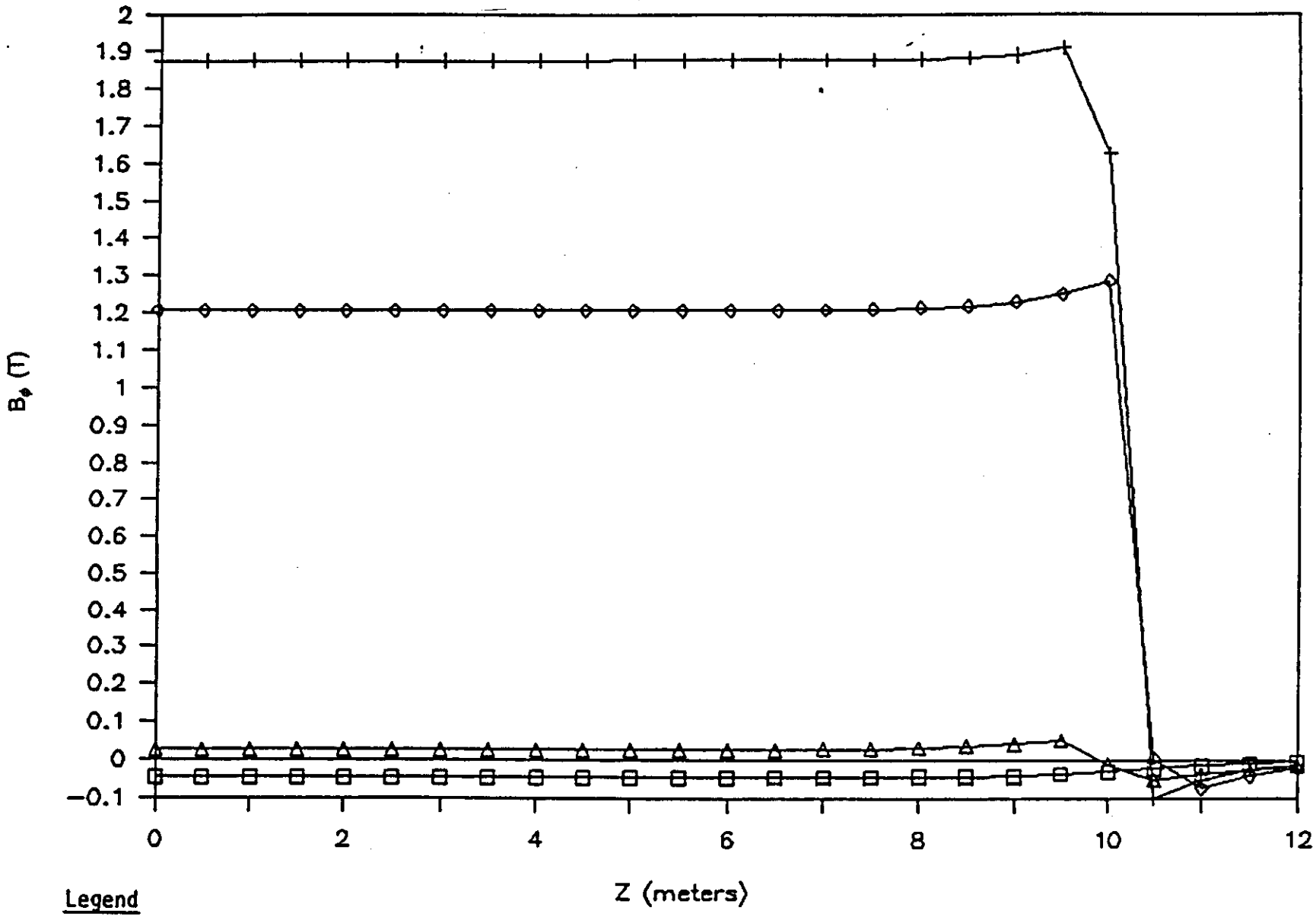

Legend

- □ Radius = 2.468 m, outer leg of plug end torus
- + Radius = 3.53 m, high field surface of inner leg of central torus
- ◊ Radius = 5.203 m, along minor axis
- △ Radius = 6.876 m, along outer surface of outer leg

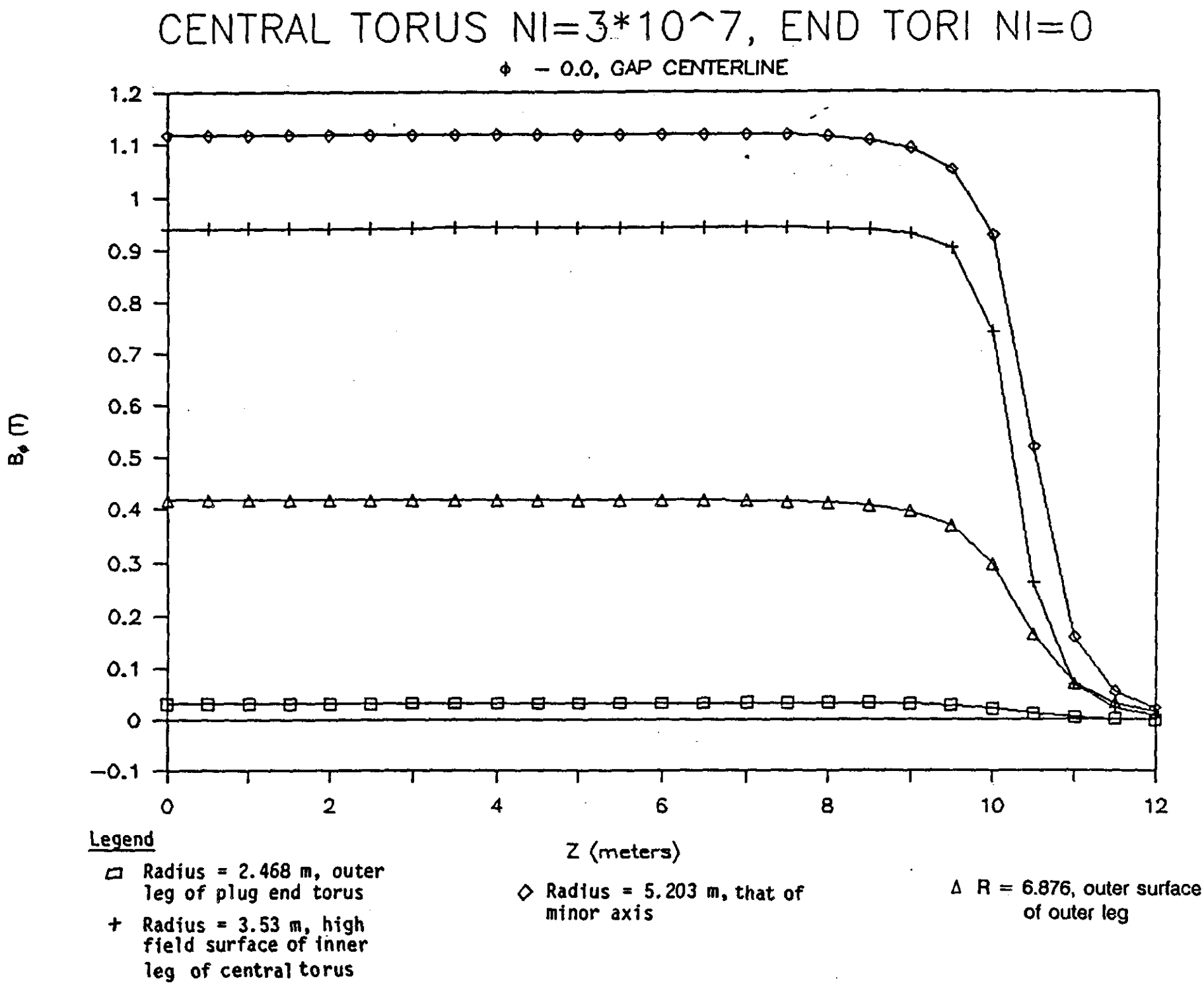
CENTRAL TORUS NI=3*10^7, END TORI NI=0
Φ – 0.0, GAP CENTERLINE
1.2
1.1
1
0.9
0.8
0.7
0.6
0.5
0.4
0.3
0.2
0.1
0
−0.1
B_Φ (T)
0
2
4
6
8
10
12
Z (meters)
Legend
Radius = 2.468 m, outer leg of plug end torus
Radius = 3.53 m, high field surface of inner leg of central torus
Radius = 5.203 m, that of minor axis
R = 6.876, outer surface of outer leg

CENTRAL TORUS NI=3*10^7, END TORI NI=0

Z = 9.0

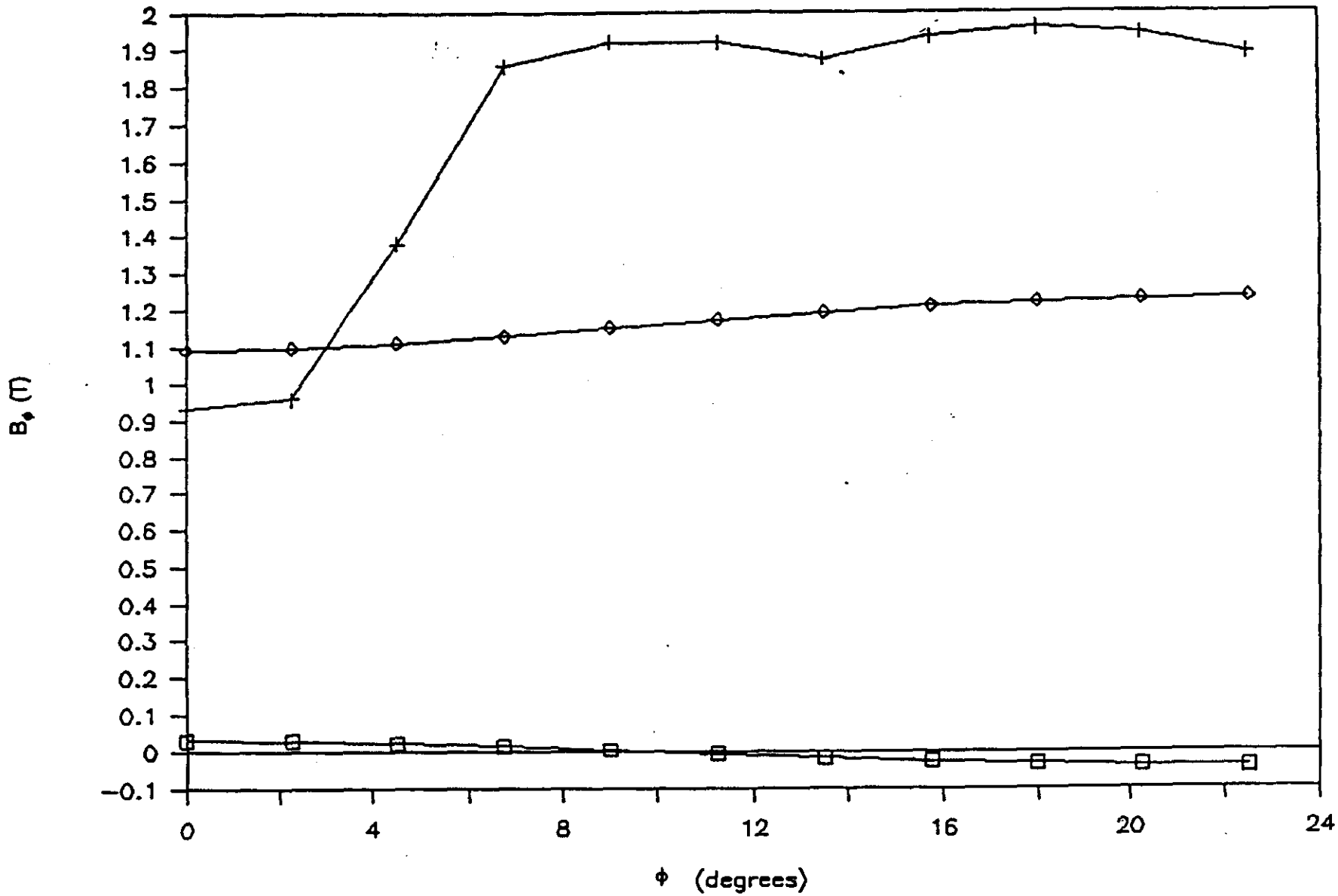

Midplane of End Torus

□ R = 2.468 ◊ 5.203

+ R = 3.53 Δ 6.876

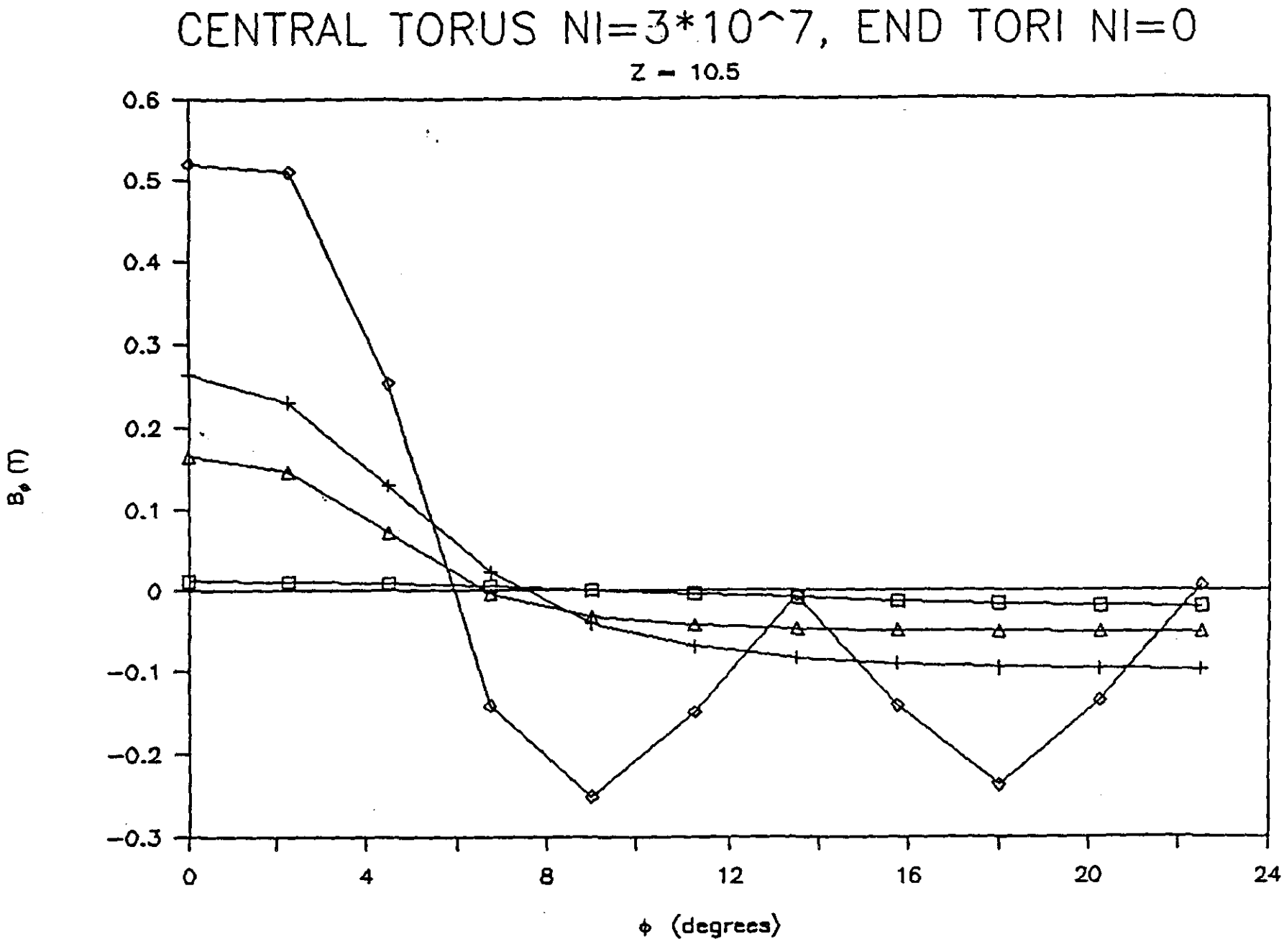

End Plane of Central Torus

□ R = 2.468 ◇ 5.203

+ R = 3.53 Δ 6.876

Appendix D

Coil and Structure Weights and Sizes

(to be supplied)

Appendix E

Cost Data - Fusion Magnets

TABLE 1: WINDING PACK LESS CONDUCTOR COST

COPPER MAGNETS	SUPERCONDUCTING MAGNETS	UNIT COSTS
TARA large plug		$ 18/kg
PLT TF		$ 27/kg
JET TF		$ 39/kg
JET PF		$ 41/kg
TARA small plug		$ 42/kg
TARA central cell		$ 50/kg
DIII PF		$ 61/kg
	MFTF - solenoids	$ 67/kg
TFTR TF		$ 76/kg
	LCP - GD (production)	$ 82/kg
DIII TF		$ 83/kg
Frascatti FTU (est.)		$ 91/kg
	Alcator DCT TF (est.)	$ 96/kg
	MFTF - Y/Y	$ 114/kg
TFTR BBC PF		$ 117/kg
	LCP - GD (repeat)	$ 121/kg
	MIT 12 T	$ 130/kg
PDX TF		$ 148/kg
TFTR - Ring PF		$ 187/kg
Zephyr TF (est.)		$ 208/kg
	LCP - W (production)	$ 248/kg
	LCP - W (repeat)	$ 420/kg

TABLE 2: WINDING PACK INCLUDING CONDUCTOR COST

COPPER MAGNETS	SUPERCONDUCTING MAGNETS	UNIT COSTS
TARA large plug		$ 26/kg
PLT TF		$ 36/kg
TARA small plug		$ 50/kg
JET TF		$ 52/kg
JET PF		$ 54/kg
TARA central cell		$ 58/kg
DIII PF		$ 71/kg
TFTR TF		$ 86/kg
DIII TF		$ 93/kg
Frascatti FTU (est.)		$ 101/kg
	MFTF solenoids	$ 105/kg
TFTR BBC PF		$ 127/kg
PDX TF		$ 148/kg
	LCP - GD (production)	$ 168/kg
TFTR Ring PF (PPL large Hum rings)		$ 197/kg
Zephyr TF (est.)		$ 218/kg
	MFTF Y/Y	$ 220/kg
	LCP - GD (repeat)	$ 246/kg
	Alcator DCT TF (est.)	$ 266/kg
	MIT 12 T	$ 336/kg
	LCP - $\overline{W}$ (production)	$ 469/kg
	LCP - $\overline{W}$ (repeat)	$ 775/kg

TABLE 3: CONDUCTOR COSTS

MAGNET	B_{max}	# GRADES	$/kA-m	$/kA-m-T
MFTF solenoids	3.3 T	1	$ 8.40	$ 2.55
MFTF Y/Y	7.8 T	1	$ 19.40	$ 2.48
LCP - GD (repeat)	8 T	3	$ 23.70	$ 2.96
Alcator DCT (est.)	10 T	1	$ 25.70	$ 2.57
MIT 12 T	10 T	1	$ 36.70	$ 3.67
LCP - W (repeat)	8 T	1	$ 34.30	$ 4.30